THE ASTROPHYSICAL JOURNAL, 553:47–72, 2001 May 20

FINAL RESULTS FROM THE *HUBBLE SPACE TELESCOPE* KEY PROJECT TO MEASURE THE HUBBLE CONSTANT[1]

WENDY L. FREEDMAN,[2] BARRY F. MADORE,[2,3] BRAD K. GIBSON,[4] LAURA FERRARESE,[5] DANIEL D. KELSON,[6] SHOKO SAKAI,[7] JEREMY R. MOULD,[8] ROBERT C. KENNICUTT, JR.,[9] HOLLAND C. FORD,[10] JOHN A. GRAHAM,[6] JOHN P. HUCHRA,[11] SHAUN M. G. HUGHES,[12] GARTH D. ILLINGWORTH,[13] LUCAS M. MACRI,[11] AND PETER B. STETSON[14,15]

Received 2000 July 30; accepted 2000 December 19

ABSTRACT

We present here the final results of the *Hubble Space Telescope* (*HST*) Key Project to measure the Hubble constant. We summarize our method, the results, and the uncertainties, tabulate our revised distances, and give the implications of these results for cosmology. Our results are based on a Cepheid calibration of several secondary distance methods applied over the range of about 60–400 Mpc. The analysis presented here benefits from a number of recent improvements and refinements, including (1) a larger LMC Cepheid sample to define the fiducial period-luminosity (PL) relations, (2) a more recent *HST* Wide Field and Planetary Camera 2 (WFPC2) photometric calibration, (3) a correction for Cepheid metallicity, and (4) a correction for incompleteness bias in the observed Cepheid PL samples. We adopt a distance modulus to the LMC (relative to which the more distant galaxies are measured) of $\mu_0(\mathrm{LMC}) = 18.50 \pm 0.10$ mag, or 50 kpc. New, revised distances are given for the 18 spiral galaxies for which Cepheids have been discovered as part of the Key Project, as well as for 13 additional galaxies with published Cepheid data. The new calibration results in a Cepheid distance to NGC 4258 in better agreement with the maser distance to this galaxy. Based on these revised Cepheid distances, we find values (in km s^{-1} Mpc^{-1}) of $H_0 = 71 \pm 2$ (random) ± 6 (systematic) (Type Ia supernovae), $H_0 = 71 \pm 3 \pm 7$ (Tully-Fisher relation), $H_0 = 70 \pm 5 \pm 6$ (surface brightness fluctuations), $H_0 = 72 \pm 9 \pm 7$ (Type II supernovae), and $H_0 = 82 \pm 6 \pm 9$ (fundamental plane). We combine these results for the different methods with three different weighting schemes, and find good agreement and consistency with $H_0 = 72 \pm 8$ km s^{-1} Mpc^{-1}. Finally, we compare these results with other, global methods for measuring H_0.

Subject headings: Cepheids — cosmology: observations — distance scale — galaxies: distances and redshifts

1. INTRODUCTION

In standard big bang cosmology, the universe expands uniformly; and locally, according to the Hubble law, $v = H_0 d$, where v is the recession velocity of a galaxy at a distance d, and H_0 is the Hubble constant, the expansion rate at the current epoch. More than seven decades have now passed since Hubble (1929) initially published the correlation between the distances to galaxies and their recession velocities, thereby providing evidence for the expansion of the universe. But pinning down an accurate value for the Hubble constant has proved extremely challenging. There are many reasons for this difficulty, but primary among them is the basic difficulty of establishing accurate distances over cosmologically significant scales.

The Hubble constant enters in a practical way into numerous cosmological and astrophysical calculations. Its inverse, H_0^{-1}, sets the age of the universe, t_0, and the size of the observable universe, $R_{\mathrm{obs}} = ct_0$, given a knowledge of the total energy density of the universe. The square of the Hubble constant relates the total energy density of the universe to its geometry (Kolb & Turner 1990; Peacock 1999). In addition, the Hubble constant defines the critical density of the universe, $\rho_{\mathrm{crit}} = (3H^2)/(8\pi G)$. The critical density further specifies the epoch in the universe at which the density of matter and radiation were equal, so that the growth of structure in the universe is also dependent on the expansion rate. The determination of many physical properties of galaxies and quasars (e.g., mass, luminosity, energy density) all require knowledge of the Hubble constant, as does the proportion of primordial light elements (H, D, ^{3}He, ^{4}He, and Li) synthesized in the first few minutes after the big bang.

Measuring an accurate value of H_0 was one of the motivating reasons for building the NASA/ESA *Hubble Space Telescope* (*HST*). Thus, in the mid 1980s, measurement of H_0 with the goal of 10% accuracy was designated as one of

[1] Based on observations with the NASA/ESA *Hubble Space Telescope*, obtained at the Space Telescope Science Institute, which is operated by AURA, Inc., under NASA contract NAS5-26555.

[2] The Observatories, Carnegie Institution of Washington, Pasadena, CA 91101.

[3] NASA/IPAC Extragalactic Database, California Institute of Technology, Pasadena, CA 91125.

[4] Centre for Astrophysics and Supercomputing, Swinburne University of Technology, Hawthorn, Victoria 3122, Australia.

[5] Rutgers University, New Brunswick, NJ 08854.

[6] Department of Terrestrial Magnetism, Carnegie Institution of Washington, 5241 Broad Branch Road NW, Washington, DC 20015.

[7] National Optical Astronomy Observatories, PO Box 26732, Tucson, AZ 85726.

[8] Research School of Astronomy and Astrophysics, Australian National University, Weston Creek Post Office, Weston, ACT, Australia 2611.

[9] Steward Observatory, University of Arizona, Tucson, AZ 85721.

[10] Department of Physics and Astronomy, Bloomberg 501, Johns Hopkins University, 3400 North Charles Street, Baltimore, MD 21218.

[11] Harvard-Smithsonian Center for Astrophysics, 60 Garden Street, Cambridge, MA 02138.

[12] Institute of Astronomy, Madingley Road, Cambridge CB3 0HA, UK.

[13] Lick Observatory, University of California, Santa Cruz, CA 95064.

[14] Dominion Astrophysical Observatory, Herzberg Institute of Astrophysics, National Research Council, 5071 West Saanich Road, Victoria, BC V8X 4M6, Canada.

[15] Guest User, Canadian Astronomy Data Centre, which is operated by the Herzberg Institute of Astrophysics, National Research Council of Canada.

three "Key Projects" of the *HST*, and teams from the astronomical community were encouraged to propose to undertake these initiatives.[16] A team headed by the late Marc Aaronson began preparing our proposal in 1984; following peer review (subsequent to the *Challenger* explosion in 1986), our group was awarded the Key Project on the Extragalactic Distance Scale in 1986. Very sadly, Marc met a tragic and untimely death in 1987. We began our initial observations of the closest galaxies in our sample in 1991, shortly after the launch of *HST*, but most of the project was carried out after the refurbishment mission (in 1993 December), when a new camera with optics that corrected for the spherical aberration of the primary mirror was installed.

The overall goal of the H_0 Key Project (hereafter simply the Key Project) was to measure H_0 based on a Cepheid calibration of a number of independent, secondary distance determination methods. Given the history of systematic errors dominating the accuracy of distance measurements, the approach we adopted was to avoid relying on a single method alone, and instead to average over the systematics by calibrating and using a number of different methods. Determining H_0 accurately requires the measurement of distances far enough away that both the small- and large-scale motions of galaxies become small compared to the overall Hubble expansion. To extend the distance scale beyond the range of the Cepheids, a number of methods that provide relative distances were chosen. We have used the *HST* Cepheid distances to provide an absolute distance scale for these otherwise independent methods, including the Type Ia supernovae, the Tully-Fisher relation, the fundamental plane for elliptical galaxies, surface brightness fluctuations, and Type II supernovae.

The previous 29 papers in this series have provided the distances to individual galaxies based on the discovery and measurement of Cepheids, discussed the calibration of the data, presented interim results on the Hubble constant, and provided the calibration of secondary methods, along with their individual determinations of the Hubble constant. A recent paper by Mould et al. (2000a) combines the results for secondary methods (Gibson, Maloney, & Sakai 2000a; Ferrarese et al. 2000a; Kelson et al. 2000; Sakai et al. 2000) with a weighting scheme based on numerical simulations of the uncertainties. In this paper, we present the final, combined results of the Key Project. This analysis benefits from significant recent refinements and improvements to the Cepheid period-luminosity relation, as well as the *HST* WFPC2 photometric scale, and puts all of the data for the Key Project and other efforts onto a new common zero point. Establishing plausible limits for the Hubble constant requires a careful investigation of systematic errors. We explicitly note where current limits in accuracy have been reached. We intend this paper to provide an assessment of the status of the global value of H_0.

In this paper, we summarize our method and determination of Cepheid distances in § 2 and § 3. In § 4 and § 5, we apply a correction for the nearby flow field and compare the value of H_0 obtained locally with that determined at greater distances. Secondary methods and the determination of H_0 on large scales are discussed in § 6 and § 7. The remaining sources of uncertainty in the extragalactic distance scale and determination of H_0 are discussed in § 8. In § 9 we compare our results to methods that can be applied directly at high redshifts, specifically the Sunyaev-Zeldovich and gravitational lensing techniques. In § 10, we give the implications of these results for cosmology.

[16] The other two Key Projects selected were Quasar Absorption Lines and the Medium-Deep Survey.

2. DESCRIPTION OF THE KEY PROJECT

2.1. *Goals*

The main aims of the Key Project were (Aaronson & Mould 1986; Freedman et al. 1994a; Kennicutt, Freedman, & Mould 1995) (1) to use the high resolving power of *HST* to discover Cepheids in, and determine distances to, a sample of nearby ($\lesssim$20 Mpc) galaxies, and establish an accurate local distance scale; (2) to determine H_0 by applying the Cepheid calibration to several secondary distance indicators operating farther out in the Hubble flow; (3) to intercompare the Cepheid and other distances to provide estimates of the external uncertainties for all the methods; and (4) to conduct tests of the universality of the Cepheid period-luminosity relation, in particular as a function of metal abundance. Finally, an ancillary aim was to measure Cepheid distances to a small number of galaxies in each of the two nearest clusters (Virgo and Fornax) as an independent check on other Hubble constant determinations.

Why was *HST* necessary for an accurate determination of H_0? Atmospheric seeing sets the practical limit for resolving Cepheids and measuring well-defined period-luminosity relations to only a few megaparsecs. The superb and essentially nonvarying image quality of *HST* extends that limit tenfold, and the effective search volume a thousandfold. Furthermore, *HST* offers a unique capability in that it can be scheduled optimally to facilitate the discovery of Cepheid variables. Observations can be scheduled independently of the phase of the Moon, the time of day, or weather, and there are no seeing variations. Before the launch of *HST*, most Cepheid searches were confined to our own Local Group of galaxies and the very nearest surrounding groups (M101, Sculptor, and M81 groups; see Madore & Freedman 1991; Jacoby et al. 1992). At that time, only five galaxies with well-measured Cepheid distances provided the absolute calibration of the Tully-Fisher relation (Freedman 1990) and a single Cepheid distance, that for M31, provided the calibration for the surface brightness fluctuation method (Tonry 1991). Moreover, before *HST no* Cepheid calibrators were available for Type Ia supernovae (although one historical, nearby Type Ia supernova, SN 1885A, had been observed in M31).

2.2. *Choice of Target Galaxies and Observing Strategy*

In each nearby target spiral galaxy in the Key Project sample, Cepheid searches were undertaken in regions active in star formation, but low in apparent dust extinction, based on ground-based, photographic images (e.g., Sandage & Bedke 1988). To the largest extent possible, we avoided high surface brightness regions in order to minimize source confusion or crowding. For each galaxy, over a 2 month time interval, *HST* images in the visual (V band, 5550 Å), and in the near-infrared (I band, 8140 Å), were made using the corrected Wide Field and Planetary Camera 2 (WFPC2). Among the galaxies on the Key Project observing program, only M81 and an outer field in M101 were observed with the original Wide Field/Planetary camera (WF/PC), before the first *HST* servicing mission that re-

TABLE 1

NUMBERS OF CEPHEID CALIBRATORS FOR SECONDARY METHODS

Secondary Method	σ (%)	N (pre-*HST*)	σ_{mean} (%)	N (post-*HST*)	σ_{mean} (%)
Tully-Fisher relation	± 20[a]	5[b]	± 10	21	± 5
Type Ia supernovae	± 8[c]	0	n/a	6[d]	± 4
Surface brightness fluctuations	± 9[e]	1	± 9	6	± 4
Fundamental plane	± 14	0	n/a	3[f]	± 10
Type II supernovae	± 12[g]	1	± 12	4	± 6

[a] Giovanelli et al. 1997.
[b] M31, M33, NGC 2403, M81, NGC 300; Freedman 1990.
[c] Hamuy et al. 1996.
[d] Using the distances to the host galaxies to SN 1937C, 1972E, 1981B, 1989B, 1990N, and 1998bu, but excluding 1895B, 1960F, 1974G.
[e] Tonry et al. 1997.
[f] Calibration based on Cepheid distances to Leo I group, Virgo and Fornax Clusters.
[g] This paper; Schmidt et al. 1994 distant clusters.

stored the telescope capabilities. Two of the Type Ia supernova calibrators investigated by the Sandage et al. team and rediscussed here were also observed with WF/PC: IC 4182 and NGC 5253. The field of view of the WFC2 is L-shaped, with each of the three cameras covering 1.′33 × 1.′33 on the sky, and the PC 35″ × 35″.

For the observations, two wavelength bands were chosen to enable corrections for dust extinction, following the precepts of Freedman (1988) and Madore & Freedman (1991). Initially, during the observing window, 12 epochs at V (F555W) and four observations at I (F814W) were obtained. For some of the galaxies observed early in the program, some B (F439W) data were also obtained. For the targets observed later in the program, observations were obtained at both V and I at each of the 12 epochs. An additional observation was generally made one year earlier or later, to increase the time baseline and reduce aliasing errors, particularly for the longer period stars. The time distribution of the observations was set to follow a power law, enabling the detection and measurement of Cepheids with a range of periods optimized for minimum aliasing between 10 and 50 days (Freedman et al. 1994b).

Since each individual secondary method is likely to be affected by its own (independent) systematic uncertainties, to reach a final overall uncertainty of $\pm 10\%$, the numbers of calibrating galaxies for a given method were chosen initially so that the final (statistical) uncertainty on the zero point for that method would be only $\sim 5\%$. (In practice, however, some methods end up having higher weight than other methods, owing to their smaller intrinsic scatter, as well as how far out into the Hubble flow they can be applied; see § 7). In Table 1, each method is listed with its mean dispersion, the numbers of Cepheid calibrators pre- and post-*HST*, and the standard error of the mean. (We note that the fundamental plane for elliptical galaxies cannot be calibrated directly by Cepheids; this method was not included in our original proposal, and it has the largest uncertainties. As described in § 6.3, it is calibrated by the Cepheid distances to three nearby groups and clusters.) The calibration of Type Ia supernovae was part of the original Key Project proposal, but time for this aspect of the program was awarded to a team led by Allan Sandage.

For the Key Project, Cepheid distances were obtained for 17 galaxies chosen to provide a calibration for secondary methods and a determination of H_0. These galaxies lie at distances between 3 and 25 Mpc. They are located in the general field, in small groups (for example, the M81 and the Leo I groups at 3 and 10 Mpc, respectively), and in major clusters (Virgo and Fornax). An additional target, the nearby spiral galaxy M101, was chosen to enable a test of the effects of metallicity on the Cepheid period-luminosity relation. *HST* has also been used to measure Cepheid distances to six galaxies targeted specifically to be useful for the calibration of Type Ia supernovae (e.g., Sandage et al.

TABLE 2

LIST OF CEPHEID GALAXIES AND CALIBRATORS

Galaxy	Secondary Methods Calibrated by a Given Galaxy[a]
NGC 224	TF, SBF
NGC 300	...
NGC 598	TF
NGC 925	TF
NGC 1326A	FP-Fornax
NGC 1365	TF, FP-Fornax
NGC 1425	TF, FP-Fornax
NGC 2090	TF
NGC 2403	TF
NGC 2541	TF
NGC 3031	TF, SBF
NGC 3198	TF
NGC 3319	TF
NGC 3351	TF, FP-Leo
NGC 3368	TF, FP-Leo, SBF, SN Ia (1998bu)
NGC 3621	TF
NGC 3627	TF, SN Ia (1989B), SN II
NGC 4258	...
NGC 4321	FP-Virgo
NGC 4414	TF, [SN Ia (1974G)][b]
NGC 4496A	FP-Virgo, SN Ia (1960F)[b]
NGC 4535	TF, FP-Virgo
NGC 4536	TF, FP-Virgo, SN Ia (1981B)
NGC 4548	TF, FP-Virgo, SBF
NGC 4639	SN Ia, FP-Virgo (1990N)
NGC 4725	TF, SBF
NGC 5253	SN Ia (1972E)
NGC 5457	SN II
NGC 7331	TF, SBF, SN II
IC 4182	[SN Ia (1937C)]
IC 1613	...

[a] FP-Leo, FP-Virgo, and FP-Fornax denote, respectively, the galaxies in the Leo I group, and the Virgo and Fornax Clusters. The calibration of the fundamental plane is based on these group/cluster distances (§ 6.3.)
[b] Not used in Gibson et al. 2000a, or in this paper's SN Ia calibration.

1996). Finally, an *HST* distance to a single galaxy in the Leo I group, NGC 3368, was measured by Tanvir and collaborators (Tanvir et al. 1995, 1999). Subsequently and fortuitously, NGC 3368 was host to a Type Ia supernova, useful for calibrating H_0 (Jha et al. 1999; Suntzeff et al. 1999).[17]

We list the galaxies that we have used in the calibration of H_0 in Table 2, along with the methods that they calibrate. To summarize the total Cepheid calibration sample, as part of the Key Project, we have surveyed and analyzed data for 18 galaxies, in addition to reanalyzing *HST* archival data for eight galaxies observed by other groups. When these distances are combined with those for five very nearby galaxies (M31, M33, IC 1613, NGC 300, and NGC 2403), it results in a total of 31 galaxies, subsets of which calibrate individual secondary methods, as shown in Table 2.

2.3. *Key Project Archival Database*

As part of our original time allocation request for the Key Project, we proposed to provide all of our data in an archive that would be accessible to the general astronomical community. We envisaged that the Cepheid distances obtained as part of the Key Project would provide a database useful for the calibration of many secondary methods, including those that might be developed in the future. For each galaxy observed as part of the Key Project, the Cepheid positions, magnitudes, and periods are available electronically from the Key Project.[18] In addition, photometry for nonvariable stars that can be used for photometry comparisons, as well as medianed (nonphotometric) images for these galaxies, are also available. These images are also archived in NED.[19]

2.4. *Photometry*

As a means of guarding against systematic errors specifically in the data-reduction phase, each galaxy within the Key Project was analyzed by two independent groups within the team, each using different software packages: DoPHOT (Schechter, Mateo, & Saha 1993; Saha et al. 1995) and ALLFRAME (Stetson 1994, 1996). The latter software was developed specifically for the optimal analysis of data sets like those of the Key Project, consisting of large numbers of observations of a single target field. Only at the end of the data-reduction process (including the Cepheid selection and distance determinations) were the two groups' results intercompared. This "double-blind" procedure proved extremely valuable. First, it allowed us to catch simple (operator) errors. It also enabled us to provide a more realistic estimate of the external data reduction errors for each galaxy distance. The limit to the accuracy of the photometry that can be obtained in these galaxy fields is set by the sky (i.e., unresolved galaxy) background in the frames, and, ultimately, the difficulty in determining aperture corrections. Each of the two packages deals with sky determination and aperture corrections in different ways, thereby providing a means of evaluating this systematic uncertainty in the Cepheid photometry. As discussed in § 8.5, we also undertook a series of artificial star tests to better quantify the effects of crowding, and to understand the limits in each of these software packages (Ferrarese et al. 2000c).

2.5. *Calibration*

The determination of accurate distances carries with it a requirement for an accurate, absolute photometric calibration. Ultimately, the uncertainty in the Hubble constant from this effort rests directly on the accuracy of the Cepheid magnitudes themselves, and hence systematically on the CCD zero-point calibration. In view of the importance of this issue for the Key Project, we undertook our own program to provide an independent calibration of both the WF/PC and WFPC2 zero points, complementary to the efforts of the teams who built these instruments and the Space Telescope Science Institute. These calibrations have been described in Freedman et al. (1994b) and Kelson et al. (1996) for WF/PC and Hill et al. (1998), Stetson (1998), and Mould et al. (2000a) for WFPC2.

As part of an *HST* program to study Galactic globular clusters, but also extremely valuable for the photometric calibration of WFPC2, hundreds of images of ω Cen, NGC 2419, and M92 have been obtained both on the ground and with *HST* over the last several years (Stetson 1998; Mould et al. 2000a). Despite this extensive effort, the calibration of WFPC2 remains a significant source of systematic uncertainty in the determination of H_0. This lingering uncertainty results from the difficulty in characterizing the charge-transfer efficiency (CTE) properties of the WFPC2, which turn out to be a complicated function of position on the chip, the brightness of the object, the brightness of the sky, and the wavelength of the observations (presumably because of the differing background levels; Stetson 1998; Whitmore, Heyer, & Casertano 1999; Saha, Labhardt, & Prosser 2000; Dolphin 2000).

Recent WFPC2 calibrations (Stetson 1998; Dolphin 2000) differ from our earlier calibration based on Hill et al. (1998). Based on the reference-star photometry published in Papers IV to XXI in the Key Project series, Mould et al. (2000a) found that the reddening-corrected distance moduli on the Stetson (1998) system were 0.07 ± 0.02 mag closer, in the mean, than those published based on the Hill et al. (1998) system. This difference in the reddening-corrected distance moduli results from a 0.02 mag mean offset in the V-band, and a 0.04 mag mean offset in the I-band. The more recent calibrations are based on a more extensive calibration data set than that available in the Hill et al. or the Saha et al. analyses, and they result in galaxy distance moduli that are closer. The main reason for this difference is that the earlier Hill et al. "long" versus "short" zero points determined for globular clusters (bright stars on faint sky) turned out to be inappropriate for the Cepheid fields (faint stars on bright sky) because the combinations of flux dependence and background dependence were different in the two situations. P. B. Stetson (2000, private communication) indicates that a 0.02–0.03 mag uncertainty remains due to this effect. The Stetson CTE correction is in agreement with Dolphin (2000) and Whitmore et al. (1999): the Stetson zero point results in reddening-corrected distance moduli that agree to within 1.5% (0.03 mag) of the new calibration by Dolphin (2000). Although Stetson did not find a significant time dependence (as seen in the more recent studies), in all

[17] In addition, recently, SN 1999by occurred in NGC 2841, a galaxy for which Cepheid observations have been taken in cycle 9 (GO-8322).

[18] For Key Project data, see: http://www.ipac.caltech.edu/H0kp/H0KeyProj.html.

[19] These can also be accessed on a galaxy-by-galaxy basis from http://nedwww.ipac.caltech.edu.

studies the temporal variation of the CTE ramps are found to be negligible for the high-background long exposures for the Key Project.

In this paper, we have adopted the WFPC2 calibration from Stetson (1998), and applied a -0.07 ± 0.04 mag correction to the reddening-corrected distance moduli. The uncertainty reflects the remaining differences in the published WFPC2 calibrations, and their impact on the distance moduli, when corrected for reddening (eqs. [3] and [4]). As we show in § 8, the uncertainty due to the WFPC2 photometric zero point remains a significant systematic error affecting the measurement of H_0. Unfortunately, until linear, well-calibrated detectors can be applied to the Key Project reference stars, this uncertainty is unlikely to be eliminated.

3. THE CEPHEID DISTANCE SCALE

The Cepheid period-luminosity relation remains the most important of the primary distance indicators for nearby galaxies. The strengths and weaknesses of Cepheids have been reviewed extensively (e.g., Feast & Walker 1987; Madore & Freedman 1991; Jacoby et al. 1992; Freedman & Madore 1996; Tanvir 1999). However, since the Cepheid distance scale lies at the heart of the H_0 Key Project, we summarize both its advantages and disadvantages briefly here again.

The strengths of Cepheids are, of course, many: they are among the brightest stellar indicators, and they are relatively young stars, found in abundance in spiral galaxies. Thus, many independent objects can be observed in a single galaxy. Their large amplitudes and characteristic (sawtooth) light curve shapes facilitate their discovery and identification; they also have long lifetimes, and hence can be reobserved at other times and other wavelengths (unlike supernovae, for example). The Cepheid period-luminosity relation has a small scatter (e.g., in the I band, the dispersion amounts to only $\sim \pm 0.1$ mag: Udalski et al. 1999). Moreover, Cepheids have been studied and theoretically modeled extensively; the reason for their variability is well understood to be a consequence of pulsation of the atmosphere, resulting from a thermodynamic, valvelike driving mechanism as (primarily) helium is cycled from a singly to doubly ionized state, and the opacity increases with compression.

There are also difficulties associated with measuring Cepheid distances. First, since Cepheids are young stars, they are found in regions where there is dust scattering, absorption, and reddening. Corrections must be made for extinction, requiring assumptions about the universal behavior of Cepheids at different wavelengths, and about the universality of the Galactic extinction law. Extinction is systematic, and its effects must either be removed by multicolor data or minimized by observing at long wavelengths, or both. Second, the dependence of the PL relation on chemical composition (metallicity) has been very difficult to quantify. Third, an accurate geometric calibration of the PL relation, at any given metallicity, has not yet been established. Fourth, as the distance of the galaxy increases (and the resolution decreases), finding and measuring individual Cepheids becomes increasingly difficult because of crowding effects. Finally, the reach of Cepheids is currently (with *HST*) confined to spiral galaxies with distances less than about 30 Mpc. Hence, Cepheids alone cannot be observed at sufficient distances to determine H_0 directly, and an accurate determination of H_0 requires an extension to other methods.

3.1. *Adopted Method for Measuring Cepheid Distances*

The application of the PL relation for the Key Project follows the procedure developed in Freedman (1988) and extended in Freedman, Wilson, & Madore (1991). The Large Magellanic Cloud (LMC) PL relation has been used as fiducial, and a distance modulus of $\mu_0 = 18.50$ mag (a distance of 50 kpc) and a mean reddening of $E(V-I) = 0.13$ [$E(B-V) = 0.10$] mag (Madore & Freedman 1991) have been adopted. The LMC V- and I-band PL relations are fitted by least-squares to the target spiral data to determine apparent distance moduli in each band. A reddening-corrected distance modulus and differential absorption with respect to the LMC are obtained using a ratio of total-to-selective absorption $R = A_V/(A_V - A_I) = 2.45$ (e.g., Cardelli, Mathis, & Clayton 1989). This procedure is equivalent to defining a reddening-free index $W = V - R(V - I)$ (Madore 1982; Freedman 1988; Freedman et al. 1991).

3.2. *Effect of Metallicity on the Cepheid Period-Luminosity Relation*

A long-standing uncertainty in the Cepheid distance scale has been the possibility that the zero point of the PL relation is sensitive to chemical composition (Freedman & Madore 1990 and references therein). It is only within the last decade or so that major observational efforts to address the metallicity issue for Cepheids have been undertaken. Accurately establishing the size of a metallicity effect for Cepheids alone has proven to be very challenging, and the issue has not yet been definitively resolved. However, although neither the magnitude of the effect nor its wavelength dependence have yet been firmly established, the observational and theoretical evidence for an effect is steadily growing. Published empirical values for the index γ (see eq. [5] in § 3.3 below) range from 0 to -1.3 mag dex^{-1} (with most values between 0 and -0.4), but these published values have been derived using a variety of different combinations of bandpasses. Since the effects of metallicity are wavelength dependent, it is critical that the appropriate correction for a given data set be applied.

Some recent theoretical models (e.g., Chiosi, Wood, & Capitanio 1993; Sandage, Bell, & Tripicco 1999; Alibert et al. 1999; Bono et al. 1999, 2000) suggest that at the VI bandpasses of the Key Project, the effect of metallicity is small, $\gamma_{VI} \sim -0.1$ mag dex^{-1}. Unfortunately, the sign of the effect is still uncertain. For example, Caputo et al. (2000) find a slope of 0.27 mag dex^{-1}, with the opposite sign. Thus, for the present, calibrating the metallicity effect based on models alone is not feasible.

A differential, empirical test for the effects of metallicity on the Cepheid distance scale was first carried out by Freedman & Madore (1990) for the nearby galaxy M31. As part of the Key Project, we carried out a second differential test comparing two fields in the face-on galaxy M101 (Kennicutt et al. 1998). These two studies are consistent with there being a shallow metallicity dependence, but the statistical significance of each test is individually low. As a follow-up to the optical study, H-band NICMOS observations have been obtained for the two fields previously observed in the optical in M101 (Macri et al. 2001). A comparison of the VIH photometry for the inner and outer fields is consistent with a metallicity sensitivity of the PL

relations, but artificial star tests in the inner field indicate that crowding is significant, and precludes an accurate determination of the magnitude of the effect. Other recent studies (e.g., Sasselov et al. 1997; Kochanek 1997) conclude that a metallicity effect is extant, and all of the empirical studies agree on the sign, if not the magnitude of the effect. Considering all of the evidence currently available and the (still considerable) uncertainties, we therefore adopt $\gamma_{VI} = -0.2 \pm 0.2$ mag dex^{-1}, approximately the midrange of current empirical values, and correct our Cepheid distances accordingly.

3.3. *Adopted Period-Luminosity Relations*

For earlier papers in this series, we adopted the slopes and zero points for the LMC V and I PL relations from Madore & Freedman (1991), based on 32 Cepheids. These PL relations are consistent with those published by Feast & Walker (1987). However, the OGLE survey has recently produced a significantly larger sample of $\sim$650 LMC Cepheids (Udalski et al. 1999). This sample has extensive phase coverage at BVI magnitudes and covers the period range of $0.4 < \log P < 1.5$. As part of the Key Project, we also undertook observations of a sample of 105 LMC Cepheids (K. Sebo et al., in preparation), and these PL relations are in very good statistical agreement with those of Udalski et al., adjusting to a common distance to the LMC. For about 60 objects common to both samples, with $P > 8$ days and having both V and I magnitudes, the offsets are -0.004 ± 0.008 mag in I and $+0.013 \pm 0.010$ mag in V (Sebo et al.). The Sebo et al. sample extends to longer periods ($\sim$40 days), and has 10 Cepheids with periods greater than 30 days, the limit of the Udalski et al. sample. These 10 Cepheids are all well fitted by, and lie within 1 σ of, the period-luminosity slopes defined by the Udalski et al. sample. The Udalski et al. data are clearly the most extensive to date, and we thus adopt their apparent PL relations as fiducial for the reanalysis in this paper.

The Udalski et al. (1999) PL calibration adopts a distance modulus of 18.2 mag, based on a distance determined using the red clump technique, whereas, as discussed above, in this paper we adopt a true distance modulus to the LMC of 18.50 mag. With this modulus and the reddening-corrected Udalski et al. Cepheid data to define the slopes and errors, our adopted M_V and M_I PL relations become

$$M_V = -2.760[\pm 0.03](\log P - 1) - 4.218[\pm 0.02] \quad (\sigma_V = \pm 0.16)\,, \tag{1}$$

$$M_I = -2.962[\pm 0.02](\log P - 1) - 4.904[\pm 0.01] \quad (\sigma_I = \pm 0.11)\,. \tag{2}$$

In the absence of a metallicity dependence, and correcting only for reddening, the true distance moduli (μ_0) can be calculated from the apparent V and I distance moduli (μ_V and μ_I) as follows:

$$\mu_0 = \mu_W = \mu_V - R(\mu_V - \mu_I) = 2.45\mu_I - 1.45\mu_V \tag{3}$$

$$= W + 3.255[\pm 0.01](\log P - 1) + 5.899[\pm 0.01] \quad (\sigma_W = \pm 0.08)\,. \tag{4}$$

As discussed in more detail in § 3.4, it is the change in slope of the I-band PL relation that has the most impact on the resulting distances.

Allowing for a correction term $\delta\mu_Z$ for a metallicity dependence of the Cepheid PL relation in terms of the observed H II region abundance of oxygen relative to hydrogen (see § 8.3), the true distance modulus becomes

$$\mu_0 = \mu_V - R(\mu_V - \mu_I) + \delta\mu_Z\,, \tag{5}$$

where $\delta\mu_Z = \gamma_{VI}([\mathrm{O/H}] - [\mathrm{O/H}]_{\mathrm{LMC}})$ is applied to the reddening-corrected (VI) modulus, and γ_{VI} is measured in mag dex^{-1} (where a dex refers to a factor of 10 difference in metallicity).

3.4. *New Revised Cepheid Distances*

Over the six years that we have been publishing data from the Key Project, our analysis methods, as well as the photometric calibration, have evolved and improved. Hence, the sample of published Key Project distances has not been analyzed completely homogeneously. In this paper, we have redetermined the true moduli to each galaxy used in the Key Project. These distances are calculated with the new calibration described above, and with attention to minimizing bias at the short-period end of the PL relation, as described below and by Freedman et al. (1994b), Kelson et al. (1996), and Ferrarese et al. (2000b).

In this analysis we have (1) consistently adopted only the published Cepheid photometry, which were reduced using the ALLFRAME stellar photometry reduction package, whose phase points were converted to mean magnitudes using intensity-weighted averages (or their template-fitted equivalents).[20] (2) To compensate for the small ($\sim$0.01 mag) mean bias in the PL fits (see the discussion in § 8.4 and Appendix A), we have also applied period cuts to the PL relations, thereby eliminating the shortest period Cepheids, where magnitude incompleteness effects become important. In two cases (NGC 3368 and NGC 300), a single long-period Cepheid was also dropped because of stochastic effects at the bright (sparsely populated) end of the PL relation, which can similarly bias solutions. The mean correction for this magnitude-limited bias is small (+1% in distance), but it is systematic, and correcting for it results in larger distances than are determined without this faint-end debiasing. (3) We have adopted a -0.07 mag correction to the Hill et al. (1998) WFPC2 calibration to be consistent with Stetson (1998) and Dolphin (2000). Finally, (4) we have adopted the published slopes of the Udalski et al. (1999) PL relations.

The adoption of the new Udalski et al. (1999) PL slopes alone has a dramatic and unanticipated effect on the previously published Cepheid distances based on the Madore & Freedman (1991) calibration. Most importantly, the change is distance dependent. The V and I PL slopes for the Madore & Freedman calibration, based on 32 stars, are -2.76 ± 0.11 and -3.06 ± 0.07, respectively. The new Udalski et al. (1999) values for these same quantities are -2.76 ± 0.03 and -2.96 ± 0.02 (eqs. [1] and [2]). Although the V-band slopes agree identically, and the I-band slopes differ by only 0.1, the impact on the derived reddenings, and therefore distances, is significant. The new calibration predicts higher reddenings, and therefore smaller distances. In addition, because of the difference in

[20] For Key Project galaxies, both phase-weighted and intensity-weighted magnitudes were generally calculated for each of the galaxies, and found to be in very good agreement. This is to be expected, since the optimal scheduling results in well-sampled phase coverage.

TABLE 3

REVISED CEPHEID DISTANCES TO GALAXIES

Galaxy (1)	μ_{old}[a] (2)	σ (3)	N_{Ceph} (4)	$\mu_{revised}$[b] (5)	σ (6)	$\mu_{P,cut}$[c] (7)	σ (8)	N^{cut}_{Ceph} (9)	Data Source (10)
NGC 224[d]	24.41	0.08	37	24.38	0.05	24.38	0.05	37	1
NGC 300[d]	26.62	0.10	16	26.53	0.07	26.53	0.07	14	2
NGC 598[d]	24.58	0.10	12	24.56	0.10	24.56	0.08	11	3
NGC 925	29.94	0.04	73	29.80	0.04	29.80	0.04	72	4
NGC 1326A.....	31.16	0.10	17	31.00	0.09	31.04	0.09	15	5
NGC 1365.....	31.38	0.05	52	31.20	0.05	31.18	0.05	47	6
NGC 1425.....	31.73	0.05	29	31.54	0.05	31.60	0.05	20	7
NGC 2090.....	30.42	0.04	34	30.27	0.04	30.29	0.04	30	8
NGC 2403[e].....	27.59	0.24	10	27.48	0.24	27.48	0.24	10	9
NGC 2541.....	30.43	0.07	34	30.26	0.07	30.25	0.05	29	10
NGC 3031.....	27.75	0.07	25	27.67	0.07	27.75	0.08	17	11
NGC 3198.....	30.80	0.08	42	30.64	0.08	30.68	0.08	36	12
NGC 3319.....	30.79	0.09	33	30.64	0.09	30.64	0.09	33	13
NGC 3351.....	30.03	0.10	49	29.90	0.10	29.85	0.09	48	14
NGC 3368.....	30.10	0.08	11	29.95	0.08	29.97	0.06	9	15[f]
NGC 3621.....	29.21	0.06	69	29.06	0.06	29.08	0.06	59	16
NGC 3627.....	29.88	0.08	35	29.71	0.08	29.86	0.08	16	17[e]
NGC 4258.....	29.49	0.07	15	29.44	0.07	29.44	0.07	15	18
NGC 4321.....	30.93	0.07	52	30.75	0.07	30.78	0.07	42	19
NGC 4414.....	31.37	0.09	9	31.18	0.09	31.10	0.05	8	20
NGC 4496A.....	30.98	0.03	98	30.80	0.03	30.81	0.03	94	17[f]
NGC 4535.....	31.02	0.05	50	30.84	0.05	30.85	0.05	47	21
NGC 4536.....	30.95	0.04	39	30.78	0.04	30.80	0.04	35	17[e]
NGC 4548.....	31.03	0.05	24	30.88	0.05	30.88	0.05	24	22
NGC 4639.....	31.80	0.07	17	31.59	0.07	31.61	0.08	14	17[f]
NGC 4725.....	30.50	0.06	20	30.33	0.06	30.38	0.06	15	17[e]
NGC 5253.....	27.60	0.10	7	27.54	0.10	27.56	0.14	4	17[f]
NGC 5457.....	29.35	0.10	29	29.18	0.10	29.13	0.11	25	23
NGC 7331.....	30.90	0.09	13	30.81	0.09	30.81	0.09	13	24
IC 4182	28.36	0.06	18	28.26	0.05	28.28	0.06	16	17[f]
IC 1613	24.29	0.14	10	24.24	0.14	24.19	0.15	9	25[f]

[a] Adopting Madore & Freedman 1991 PL slopes; LMC distance modulus 18.50; ALLFRAME intensity-weighted mean magnitudes or Stetson template fits if available; Hill et al. 1998 calibration, except for M31 (NGC 224), M33 (NGC 598), IC 1613, NGC 300, NGC 2403, M81 (NGC 3031), and M101 (outer; NGC 5457).

[b] Adopting Udalski et al. 1999 PL slopes; same Cepheid sample as for col. (2); Stetson 1998 WFPC2 calibration, except for M31, M33, IC 1613, NGC 300, NGC 2403, and M81. (To transform distance moduli from Hill et al. to Stetson, 0.07 mag is subtracted.)

[c] Same calibration as for col. (5), but applying a period cut at the short-period end to minimize bias in the period-luminosity relation; where the numbers of Cepheids in cols. (4) and (9) are equal, no period cut was applied.

[d] For the galaxies M31, M33, and NGC 300, observed from the ground, and for which *BVRI* photometry are available, distances tabulated here are based on *VI* photometry to be consistent with the *HST* sample galaxies.

[e] *I*-band data are only available for NGC 2403. A reddening of $E(V-I) = 0.20 \pm 0.10$ has been adopted, comparable to that for other spiral galaxies; see Table 4.

[f] Reanalyzed by Gibson et al. 2000a.

REFERENCES.—(1) Freedman & Madore 1990; (2) Freedman et al. 1992; (3) Freedman et al. 1991; (4) Silbermann et al. 1996; (5) Prosser et al. 1999; (6) Silbermann et al. 1999; (7) Mould et al. 2000b; (8) Phelps et al. 1998; (9) Freedman & Madore 1988; (10) Ferrarese et al. 1998; (11) Freedman et al. 1994; (12) Kelson et al. 1999; (13) Sakai et al. 1999; (14) Graham et al. 1997; (15) Tanvir et al. 1995; (16) Rawson et al. 1997; (17) Gibson et al. 1999; (18) Newman et al. 2001; (19) Ferrarese et al. 1996; (20) Turner et al. 1998; (21) Macri et al. 1999; (22) Graham et al. 1999; (23) Kelson et al. 1996; (24) Hughes et al. 1998; (25) Freedman 1988.

$(V-I)$ slope, the new relation predicts systematically larger reddenings for Cepheids of increasing period. As a result, the differences in distance between the previous and the new calibration will be largest for galaxies at greater distances, where the mean period of the samples is larger (since a greater fraction of shorter period Cepheids will fall below the detection threshold in the most distant targets).

Expressing the divergence of the two calibrations as a correction to the true modulus (in the sense of Udalski et al. 1999 minus Madore & Freedman 1991),

$$\Delta\mu_0 = -0.24(\log P - 1.0) \text{ mag} . \quad (6)$$

The two calibrations agree at around 10 days in period. At 20 days the correction amounts to less than a 4% decrease in distance. At 30 days, this difference is 6%, and it rises to 9.5% (or -0.19 mag in distance modulus) at 60 days.

In Table 3, this new calibration is applied to all KP galaxies and other Cepheid distances from *HST* observations. Corrections for metallicity are applied in Table 4. In addition, we present revised *VI* moduli for M33, M31, IC 1613, NGC 300, and *I*-band for NGC 2403. These galaxies were previously observed from the ground, and with the exception of IC 1613 (which was observed with NICMOS), have also been used as calibrators for secondary methods for the

TABLE 4

FINAL ADOPTED DISTANCE MODULI, REDDENINGS, DISTANCES, METALLICITIES

Galaxy (1)	μ_V (mag) (2)	σ_V[a] (3)	μ_I (mag) (4)	σ_I[a] (5)	$E(V-I)$ (mag) (6)	$\sigma_{E(V-I)}$ (mag) (7)	μ_0 (mag) (8)	σ_0[a] (9)	D_0 (Mpc) (10)	μ_Z (mag) (11)	D_Z (Mpc) (12)	Z[b] (dex) (13)	σ_Z[a] (dex) (14)
NGC 224	25.01	0.07	24.76	0.05	0.26	0.04	24.38	0.05	0.75	24.48	0.79	8.98	0.15
NGC 300	26.60	0.05	26.57	0.04	0.04	0.03	26.53	0.07	2.02	26.50	2.00	8.35	0.15
NGC 598	25.21	0.11	24.94	0.08	0.27	0.05	24.56	0.10	0.82	24.62	0.84	8.82	0.15
NGC 925	30.33	0.04	30.12	0.03	0.21	0.02	29.80	0.04	9.12	29.81	9.16	8.55	0.15
NGC 1326A.....	31.41	0.07	31.26	0.07	0.15	0.04	31.04	0.10	16.14	31.04	16.14	8.50	0.15
NGC 1365.....	31.69	0.05	31.49	0.04	0.20	0.02	31.18	0.05	17.22	31.27	17.95	8.96	0.20
NGC 1425.....	32.01	0.07	31.85	0.05	0.16	0.03	31.60	0.05	20.89	31.70	21.88	9.00	0.15
NGC 2090.....	30.71	0.05	30.54	0.04	0.17	0.02	30.29	0.04	11.43	30.35	11.75	8.80	0.15
NGC 2403.....	...	...	27.75	0.10	0.2[c]	0.1	27.48	0.10	3.13	27.54	3.22	8.80	0.10
NGC 2541.....	30.74	0.05	30.54	0.04	0.20	0.02	30.25	0.05	11.22	30.25	11.22	8.50	0.15
NGC 3031.....	28.22	0.09	28.03	0.07	0.19	0.05	27.75	0.08	3.55	27.80	3.63	8.75	0.15
NGC 3198.....	31.04	0.05	30.89	0.04	0.15	0.04	30.68	0.08	13.68	30.70	13.80	8.60	0.15
NGC 3319.....	30.95	0.06	30.82	0.05	0.13	0.04	30.64	0.09	13.43	30.62	13.30	8.38	0.15
NGC 3351.....	30.43	0.06	30.19	0.05	0.24	0.04	29.85	0.09	9.33	30.00	10.00	9.24	0.20
NGC 3368.....	30.44	0.11	30.25	0.08	0.20	0.04	29.97	0.06	9.86	30.11	10.52	9.20	0.20
NGC 3621.....	29.97	0.07	29.61	0.05	0.36	0.04	29.08	0.06	6.55	29.11	6.64	8.75	0.15
NGC 3627.....	30.44	0.09	30.20	0.07	0.24	0.03	29.86	0.08	9.38	30.01	10.05	9.25	0.15
NGC 4258.....	29.99	0.08	29.77	0.05	0.22	0.04	29.44	0.07	7.73	29.51	7.98	8.85	0.15
NGC 4321.....	31.31	0.06	31.09	0.05	0.22	0.03	30.78	0.07	14.32	30.91	15.21	9.13	0.20
NGC 4414.....	31.48	0.14	31.33	0.10	0.15	0.04	31.10	0.05	16.60	31.24	17.70	9.20	0.15
NGC 4496A.....	31.14	0.03	31.00	0.03	0.14	0.01	30.81	0.03	14.52	30.86	14.86	8.77	0.15
NGC 4535.....	31.32	0.04	31.13	0.04	0.19	0.02	30.85	0.05	14.79	30.99	15.78	9.20	0.15
NGC 4536.....	31.24	0.04	31.06	0.04	0.18	0.02	30.80	0.04	14.45	30.87	14.93	8.85	0.15
NGC 4548.....	31.30	0.07	31.12	0.04	0.18	0.04	30.88	0.05	15.00	31.05	16.22	9.34	0.15
NGC 4639.....	31.96	0.09	31.84	0.07	0.12	0.04	31.61	0.08	20.99	31.71	21.98	9.00	0.15
NGC 4725.....	31.08	0.08	30.79	0.07	0.29	0.03	30.38	0.06	11.91	30.46	12.36	8.92	0.15
NGC 5253.....	28.01	0.17	27.83	0.12	0.19	0.08	27.56	0.14	3.25	27.49	3.15	8.15	0.15
NGC 5457[d]	29.46	0.07	29.33	0.05	0.13	0.06	29.13	0.11	6.70	29.13	6.70	8.50	0.15
NGC 7331.....	31.42	0.09	31.17	0.06	0.25	0.05	30.81	0.09	14.52	30.84	14.72	8.67	0.15
IC 4182	28.37	0.07	28.33	0.06	0.04	0.03	28.28	0.06	4.53	28.26	4.49	8.40	0.20
IC 1613	24.44	0.09	24.34	0.10	0.10	0.05	24.19	0.15	0.69	24.06	0.65	7.86	0.50

[a] Random uncertainty, not including systematic errors.
[b] 12 + log (O/H) (Ferrarese et al. 2000b).
[c] Adopted reddening; see text.
[d] The distance given for M101 is based on data for an outer field in this galaxy (Kelson et al. 1996), where the metallicity is very nearly that of the LMC.

Key Project. We have not included other dwarf galaxies (such as NGC 6822 or WLM) that are not calibrators for the secondary methods adopted in this paper. The fits were done using the same standard procedure described in § 3.1, and adopting equation (3). To make it clear where the differences lie compared to previous calibrations, we list in columns (1)–(4) of Table 3 the galaxies, distance moduli, errors, and number of Cepheids fitted, based on the Madore & Freedman (1991) LMC PL relations, and ALLFRAME magnitudes, for an LMC distance modulus of 18.50 mag. In columns (5) and (6), we list distance moduli and errors for fits to the same Cepheid samples adopting the Udalski et al. (1999) PL slopes. In columns (7), (8), and (9), distance moduli, errors, and the number of Cepheids fitted are given, after imposing period cuts correcting for PL bias as described above. Finally, references for the sources for the Cepheid photometry are given in column (10). In Table 4, we list the galaxy name, apparent V and I distance moduli, PL-fitting (random) errors, $E(V-I)$, and distance moduli on the new calibration for the case where no metallicity correction has been applied ($\delta\mu_Z = 0$) and where a correction of $\delta\mu_Z = -0.2$ mag dex^{-1} is adopted. In addition, we list the distance in Mpc and the metallicities for the Cepheid fields. For ease of comparison, column (7) of Table 3 and column (8) of Table 4 are the same distance moduli values, uncorrected for metallicity.

The errors on the Cepheid distances are calculated as follows. The random uncertainties, $\sigma^2_{\rm random}$, are given by

$$\sigma^2_W/(N-1)\ ,$$

where N is the number of Cepheids observed in a given galaxy. The error in W, σ^2_W, includes the random errors in the photometry minus the correlated scatter along a reddening trajectory (from eq. [3]). The systematic errors are given by

$$\sigma^2_{\rm systematic} = \sigma^2_{\rm zp} + \sigma^2_Z + \sigma^2_{\rm WFPC2} + \sigma^2_{\rm apcorr}\ ,$$

with corresponding terms due to the uncertainty in the LMC zero point, metallicity, photometric zero point, and aperture corrections. A further discussion of errors can be found in Madore et al. (1999) and Ferrarese et al. (2000b).

There are three interesting effects of the differential distance-dependent effect in adopting the new Udalski et al. (1999) calibration. First, the absolute magnitudes of the Type Ia supernovae, which previously produced lower values of the Hubble constant in comparison to the other Key Project secondary distance indicators, now come into systematically better correspondence (§ 6.1). Second,

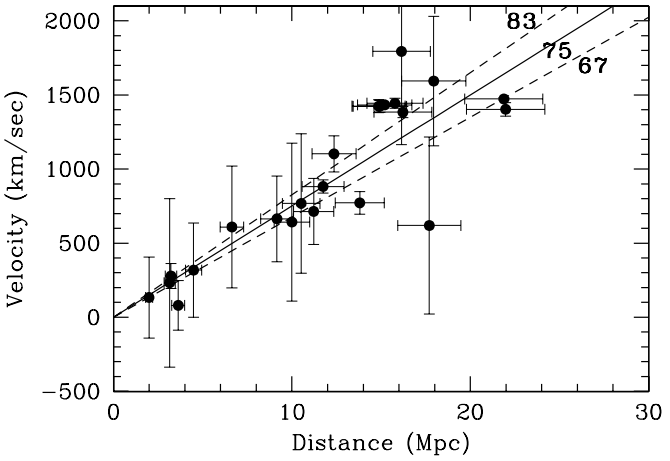

FIG. 1.—Velocity vs. distance for galaxies with Cepheid distances. Velocities in this plot have been corrected using the flow model described in Mould et al. (2000a). The Cepheid distances have been corrected for metallicity. A formal fit to these data yields a slope of $H_0 = 75 \pm 10$ (random) km s^{-1} Mpc^{-1}, in good agreement, to within the uncertainties, with the value of H_0 obtained for methods that extend to much greater distances.

another apparent divergence in the Cepheid distance scale is also ameliorated by this new calibration; that of the difference between the maser and the Cepheid distance to NGC 4258. As discussed further in § 8.1.1, adopting the Key Project fitting methodology, ALLFRAME photometry, template-fitted magnitudes, and the new calibration, the Cepheid distance to NGC 4258 comes into better agreement with the maser distance to this galaxy (Herrnstein et al. 1999). Finally, the reddening solutions for two galaxies, NGC 300 and IC 4182, previously yielded negative values. The adoption of the new Udalski et al. (1999) slopes results in positive reddening solutions for both of these (and now all) galaxies with measured Cepheid distances.

4. THE LOCAL FLOW FIELD

Before proceeding with a determination of the Hubble constant, we turn our attention to the question of the local flow field, recalling that H_0 requires a solid knowledge of both distances and velocities. The large-scale distribution of matter in the nearby universe perturbs the local Hubble flow, causing peculiar motions. If uncorrected for, these perturbations can be a significant fraction of the measured radial velocity, particularly for the nearest galaxies. The local flow field has been modeled extensively by a number of authors (e.g., Tonry et al. 2000). In general, there is good qualitative agreement among different studies. On average, these peculiar motions amount to $\sim$200–300 km s^{-1} (Tonry et al. 2000; Giovanelli et al. 1999), but the flow field is complicated locally by the presence of massive, nearby structures, most notably the Virgo Cluster. At 3000 km s^{-1}, the peculiar motion for an individual object can amount to a 7%–10% perturbation, whereas for Type Ia supernovae (which reach out to 30,000 km s^{-1}), these effects drop to less than 1%, on average.

For the nearest galaxies, the effects of the local peculiar velocity field and the resulting uncertainty in H_0 can be quite large. For example, a recent study by Willick & Batra (2000) finds values of $H_0 = 85 \pm 5$ and 92 ± 5 km s^{-1} Mpc^{-1} based on applying different local velocity models to 27 Cepheid galaxies within $\sim$20 Mpc. However, the velocity model of Han & Mould (1990) applied to 12 Cepheid distances fits best with $H_0 \sim 70$ km s^{-1} Mpc^{-1} (Mould et al. 1996). Some of this difference reflects a difference in calibration of the surface brightness fluctuation method. However, the remaining large discrepancies serve to emphasize that the Key Project strategy of extending secondary distance measurements beyond 100 Mpc, where recession

TABLE 5

LOCAL VELOCITY FLOW

Galaxy	$V_{\rm helio}$	$V_{\rm LG}$	$V_{\rm CMB}$	$V_{\rm Virgo}$	$V_{\rm GA}$	$V_{\rm Shapley}$	$V_{\rm Tonry}$
NGC 0300.....	144	125	−57	114	92	133	−140
NGC 0925.....	553	781	398	778	561	664	374
NGC 1326A.....	1836	1749	1787	1698	1742	1794	1164
NGC 1365.....	1636	1544	1597	1503	1544	1594	1157
NGC 1425.....	1512	1440	1477	1403	1417	1473	1465
NGC 2403.....	131	300	216	343	222	278	193
NGC 2541.....	559	646	736	744	674	714	936
NGC 2090.....	931	757	1057	805	869	882	926
NGC 3031.....	−34	127	65	139	43	80	246
NGC 3198.....	662	704	890	768	765	772	848
NGC 3351.....	778	641	1117	594	696	642	1175
NGC 3368.....	897	761	1236	715	823	768	1238
NGC 3621.....	805	615	1152	557	687	609	1020
NGC 4321.....	1571	1469	1856	1350	1501	1433	1436
NGC 4414.....	716	693	959	586	661	619	1215
NGC 4496A.....	1730	1575	2024	1350	1518	1424	1467
NGC 4548.....	486	381	763	1350	1460	1384	1421
NGC 4535.....	1961	1826	2248	1350	1530	1444	1410
NGC 4536.....	1804	1642	2097	1350	1521	1423	1463
NGC 4639.....	1010	902	1283	1350	1481	1403	1448
NGC 4725.....	1206	1161	1446	1040	1156	1103	1225
IC 4182	321	344	513	312	355	318	636
NGC 5253.....	404	156	612	160	349	232	800
NGC 7331.....	816	1110	508	1099	912	999	820

velocities have become large, is preferable to any local determination.

For the Key Project, we have corrected the observed galaxy velocities for the local flow field as described in Mould et al. (2000a, 2000b).[21] A linear infall model composed of three mass concentrations (the Local Supercluster, the Great Attractor, and the Shapley concentration) is constructed with parameters estimated from existing catalogs of Tully-Fisher distances and velocities. In § 8.6, we return to the question of whether there is evidence for a bulk (or nonconverging) flow on larger scales.

5. CEPHEID HUBBLE DIAGRAM

A Hubble diagram for 23 galaxies with Cepheid distances is shown in Figure 1. The galaxy velocities have been corrected for the flow-field model described above. The error bars in this plot reflect the difference between the predictions from this flow field and those of Tonry et al. (2000). A fit to the data yields a slope of 75 ± 10 km s^{-1} Mpc^{-1}, excluding systematic errors. As we show in § 7, the scatter is larger in this Hubble diagram than for the secondary methods that operate at greater distances; however, the mean value of H_0 for nearby galaxies is in very good agreement with the distant sample. In Table 5, we give the uncorrected, heliocentric velocities for the Cepheid galaxies, and the velocities as successive corrections are added: corrections for the Local Group, the Virgo cluster, the Great Attractor, and the Shapley concentration. The velocities plotted include all of these corrections. For comparison, we also list the velocities calculated from the Tonry et al. (2000) flow model, using our Cepheid distances, and assuming $H_0 = 78$ km s^{-1} Mpc^{-1} and $\Omega_m = 0.2$, as in their paper. There are some differences between the simple flow model that we have adopted and the Tonry et al. model, most significantly the Fornax Cluster galaxies. Our adopted triple-attractor model yields a quieter flow at Fornax, and reproduces the cosmic microwave background frame. The agreement for the Virgo Cluster, however, is excellent. Again, this comparison demonstrates the importance of measuring H_0 at large distances where uncertainties in the velocities become unimportant.

6. RELATIVE DISTANCE METHODS AND H_0

For the determination of H_0, a given method for measuring distances should satisfy several basic criteria (e.g., Freedman 1997): (1) It should exhibit high internal precision; (2) it should have a solid empirical calibration; (3) ideally, it should be applicable to large distances (and therefore not subject to significant systematics due to large-scale flows); and also (4) ideally, it should be based on straightforward physics. As discussed further below, based on these criteria, each of the relative distance indicators has its own merits and drawbacks. For example, Type Ia supernovae (SN Ia) have a number of advantages relative to other methods: currently they can be applied at the greatest distances ($\sim$400 Mpc), and the internal precision of this method is very high. However, finding them is difficult: supernovae are rare objects, and separating the supernova from the background light of the galaxy is challenging in the inner regions of galaxies. Moreover, for nearby galaxies, surveying for supernovae is a time-consuming process that must be done on a galaxy-by-galaxy basis. The internal precision of the surface brightness fluctuation (SBF) method is also very high, but this method currently has the most limited distance range, only $\sim$70 Mpc. Of somewhat lower internal precision is the Tully-Fisher (TF) relation, but it can be applied out to intermediate distances ($\sim$150 Mpc). The fundamental plane (FP) for elliptical galaxies can be applied, in principle, out to $z \sim 1$, but in practice, stellar evolution effects limit this method to $z \lesssim 0.1$ ($\sim$400 Mpc). Moreover, since elliptical galaxies do not contain Cepheids, the FP calibration currently relies on less direct group/cluster distances. Each of these distance indicators is now discussed briefly. The results from these methods are then combined in § 7.

6.1. *Type Ia Supernovae*

One of the most promising cosmological distance indicators is the peak brightness of Type Ia supernovae. Of long-standing interest (e.g., Kowal 1968; Sandage & Tammann 1982), this secondary indicator currently probes farther into the unperturbed Hubble flow, and possesses the smallest intrinsic scatter of any of the indicators discussed thus far. A simple lack of Cepheid calibrators prevented the accurate calibration of Type Ia supernovae prior to *HST*. Substantial improvements to the supernova distance scale have resulted from recent dedicated, ground-based supernova search and follow-up programs yielding CCD light curves (e.g., Hamuy et al. 1995, 1996; Riess et al. 1998, 1999), as well as a campaign to find Cepheids in nearby galaxies that have been host to Type Ia supernovae (Sandage et al. 1996; Saha et al. 1999).

An ALLFRAME analysis of the Cepheid distances to Type Ia supernova hosts and a comparison with the published DoPHOT results was undertaken by Gibson et al. (2000a) as part of the Key Project. Using the same pipeline reduction methods that we applied to all of the Key Project galaxies, we independently derived Cepheid distances to seven galaxies that were hosts to Type Ia supernovae. We found that on average, our new distance moduli were 0.12 ± 0.07 mag (6% in distance) smaller than those previously published (see Gibson et al., Table 4). Adopting the recalibrated distances, and applying these to the reddening-corrected Hubble relations of Suntzeff et al. (1999), Gibson et al. determined a value of $H_0 = 68 \pm 2$ (random) ± 5 (systematic) km s^{-1} Mpc^{-1}. In general, the published DoPHOT Cepheid photometry and our ALLFRAME analysis agree quite well, at or significantly better than the 1 σ level, with the I-band data tending to show poorer agreement. Thus, photometric reduction is not the major source of the difference. A variety of reasons, detailed by Gibson et al., lead to the differences in the final distance moduli.

In principle, one could average the distances determined by the two groups. However, in some cases, there are very clear-cut reasons to prefer the Gibson et al. results. For example, in the case of NGC 4536, the WFC2 chip results are discrepant (by 0.66 mag) in the Saha et al. (1996) DoPHOT analysis, whereas the Saha et al. analysis of the other three chips agrees with our ALLFRAME analysis of all four WFPC chips. Parodi et al. (2000) have attributed this difference to uncertainties in aperture corrections, and continue to prefer to average all four chips together. However, given their quoted aperture-correction uncer-

[21] Note that the signs in equation (A2) published in Mould et al. 2000a are wrong in the text; however, they were correct in the code used to do the calculations.

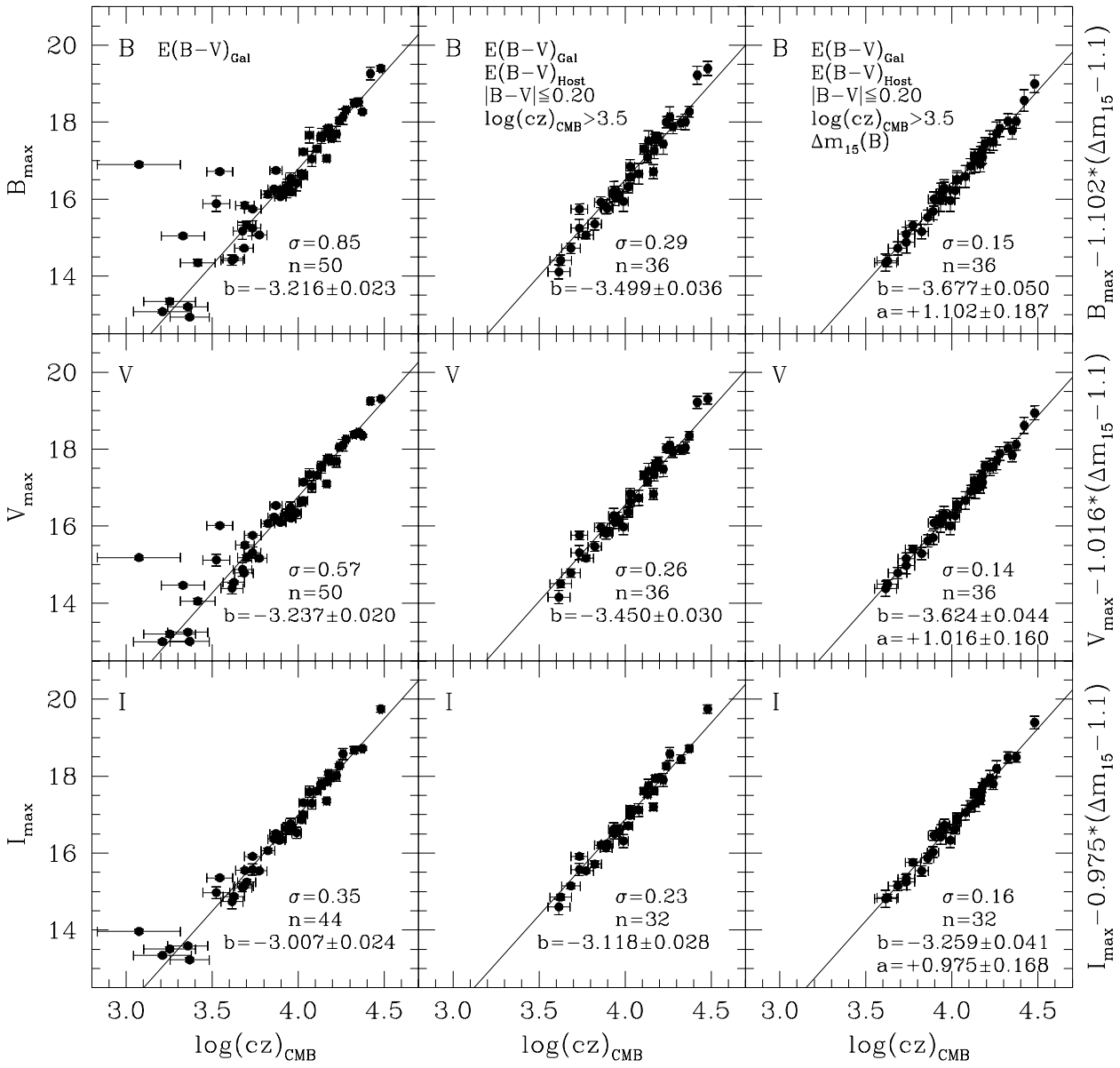

FIG. 2.—Three sets of Hubble relations constructed from the Calán-Tololo (Hamuy et al. 1996) and CfA-2 (Riess et al. 1999) Type Ia supernova samples. *Left*: The full sample of 50 supernovae, with peak magnitudes corrected only for foreground Galactic reddening. All tabulated heliocentric velocities have been corrected to the cosmic microwave background reference frame using the velocity calculator available in the NASA Extragalactic Database (NED). *Middle*: Our adopted sample of 36 supernovae, excluding those with peak $B-V$ colors in excess of 0.20 mag and velocities with respect to the cosmic microwave background below 3100 km s^{-1}. Both foreground Galactic and host galaxy reddening corrections were applied. *Right*: The Hubble relations adopted for this paper. Same as for the middle panel, but an additional correction for the light curve shape (linear in Δm_{15} [B]) has been applied. All slopes a, zero points b, and dispersions σ are noted in their relevant panels. Foreground Galactic reddening corrections $E(B-V)_{\rm Gal}$ are based on *COBE* DIRBE data (Schlegel, Finkbeiner, & Davis 1998). To retain consistency with the Key Project series of papers, we employed a ratio of total-to-selective absorption $R_V = 3.3$ and the Cardelli et al. (1989) extinction law throughout.

tainties (0.10–0.15 mag), and the fact that our analysis reveals no such difference in aperture correction, this appears to be an unlikely explanation. For the case of NGC 4639, Saha et al. (1997) introduced a different weighting scheme for that galaxy only; however, in our analysis we find no significant difference in a weighted or unweighted fit. Our preferred approach is to treat the fitting of all the galaxies and their reddening determinations in a consistent manner, rather than adopting different schemes for individual galaxies.

The supernova Hubble relation calibrated by Gibson et al. (2000a) was that of Suntzeff et al. (1999), based upon a subsample of 35 supernovae from Hamuy et al. (1996) and Riess et al. (1998). A larger total sample of nearby supernovae is now available as a result of the ongoing search program of Riess et al. (1999). In this paper, we add 21 of these additional 22 supernovae to the original Hamuy et al. sample of 29; only SN 1996ab is not considered further, since its redshift is in excess of the regime over which the Hamuy et al. (1996) k-corrections are applicable. For completeness, in the first panel of Figure 2, we show the raw, uncorrected B, V, and I Hubble diagrams for this full set of 50 supernovae.

Following Jha et al. (1999), in the middle panel of Figure 2 we show the B, V, and I Hubble diagrams for the subset of 36 supernovae having $3.5 < \log (cz)_{\rm CMB} < 4.5$, and peak

TABLE 6

TYPE IA SUPERNOVAE HUBBLE CONSTANT

Supernova	V_{CMB}	D (Mpc)	H_0^{CMB}	σ
SN 1990O	9065	134.7	67.3	2.3
SN 1990T	12012	158.9	75.6	3.1
SN 1990af	15055	198.6	75.8	2.8
SN 1991S	16687	238.9	69.8	2.8
SN 1991U	9801	117.1	83.7	3.4
SN 1991ag	4124	56.0	73.7	2.9
SN 1992J	13707	183.9	74.5	3.1
SN 1992P	7880	121.5	64.8	2.2
SN 1992ae	22426	274.6	81.6	3.4
SN 1992ag	7765	102.1	76.1	2.7
SN 1992al	4227	58.0	72.8	2.4
SN 1992aq	30253	467.0	64.7	2.4
SN 1992au	18212	262.2	69.4	2.9
SN 1992bc	5935	88.6	67.0	2.1
SN 1992bg	10696	151.4	70.6	2.4
SN 1992bh	13518	202.5	66.7	2.3
SN 1992bk	17371	235.9	73.6	2.6
SN 1992bl	12871	176.8	72.7	2.6
SN 1992bo	5434	77.9	69.7	2.4
SN 1992bp	23646	309.5	76.3	2.6
SN 1992br	26318	391.5	67.2	3.1
SN 1992bs	18997	280.1	67.8	2.8
SN 1993B	21190	303.4	69.8	2.4
SN 1993O	15567	236.1	65.9	2.1
SN 1993ag	15002	215.4	69.6	2.4
SN 1993ah	8604	119.7	71.9	2.9
SN 1993ac	14764	202.3	72.9	2.7
SN 1993ae	5424	71.8	75.6	3.1
SN 1994M	7241	96.7	74.9	2.6
SN 1994Q	8691	127.8	68.0	2.7
SN 1994S	4847	66.8	72.5	2.5
SN 1994T	10715	149.9	71.5	2.6
SN 1995ac	14634	185.6	78.8	2.7
SN 1995ak	6673	82.4	80.9	2.8
SN 1996C	9024	136.0	66.3	2.5
SN 1996bl	10446	132.7	78.7	2.7

magnitude colors $|B_{max} - V_{max}| \leq 0.20$. In addition, a correction for the internal reddening of the host galaxy, $E(B-V)_{Host}$, from Phillips et al. (1999), has been applied. In the third panel of Figure 2, our adopted subset of 36 supernovae have had their peak magnitudes corrected for their light curve shape, via application of a simple linear fit to the relation between decline rate, $\Delta m_{15}(B)$, and peak magnitude. This correction echoes that adopted in the original Hamuy et al. (1996) analysis, as opposed to the quadratic fits adopted by Phillips et al. (1999) and Gibson et al. (2000a); however, we find no difference in the result whether a linear or quadratic fit is adopted.

Adopting our default Hubble relations (Fig. 2) coupled with the zero points provided by our revised Cepheid distances (applying a metallicity correction of -0.2 ± 0.2 mag dex^{-1}) to NGC 4639, 4536, 3627, 3368, 5253, and IC 4182 from Table 4 yields a value of $H_0 = 71 \pm 2 \pm 6$ km s^{-1} Mpc^{-1}. This value can be compared to that from Gibson et al. (2000a) of $H_0 = 68 \pm 2 \pm 5$ km s^{-1} Mpc^{-1}. The difference in H_0 compared to Gibson et al. comes from the new calibration of the PL relation, a metallicity correction, and our adoption of an expanded supernovae sample. An error analysis identical to that employed by Gibson et al. was assumed here. The velocities, distances, H_0 values, and uncertainties for the 36 Type Ia supernovae used in this analysis are listed in Table 6.

6.2. *The Tully-Fisher Relation*

For spiral galaxies, the total (corrected to face-on inclination) luminosity is strongly correlated with the maximum rotation velocity of the galaxy (corrected to edge-on inclination), which is useful for measuring extragalactic distances (Tully & Fisher 1977; Aaronson et al. 1986; Pierce & Tully 1988; Giovanelli et al. 1997). The Tully-Fisher relation at present is the most commonly applied distance indicator: thousands of distances are now available for galaxies both in the general field and in groups and clusters. The scatter in this relation is approximately

TABLE 7

I-BAND TULLY-FISHER HUBBLE CONSTANT

Cluster/Group	V_{CMB}	V_{flow}	σ	D (Mpc)	H_0^{CMB}	σ	H_0^{flow}	σ
Abell 1367	6709	6845	88	89.2	75.2	12.5	76.7	12.8
Abell 0262	4730	5091	80	66.7	70.9	11.8	76.2	12.7
Abell 2634	8930	9142	79	114.9	77.7	12.4	79.6	12.7
Abell 3574	4749	4617	11	62.2	76.2	12.2	74.2	11.9
Abell 0400	7016	6983	75	88.4	79.3	12.6	79.0	12.6
Antlia	3106	2821	100	45.1	68.8	11.3	62.5	10.3
Cancer	4982	4942	80	74.3	67.1	11.0	66.5	10.9
Cen 30	3272	4445	150	43.2	75.8	12.8	102.9	17.4
Cen 45	4820	4408	100	68.2	70.7	11.9	64.6	10.9
Coma	7143	7392	68	85.6	83.5	13.4	86.4	13.9
Eridanus	1607	1627	30	20.7	77.6	12.9	78.5	13.1
ESO 50	3149	2896	100	39.5	79.8	13.0	73.3	11.9
Fornax	1380	1372	45	15.0	92.2	15.3	91.7	15.2
Hydra	4061	3881	50	58.3	69.6	11.1	66.5	10.6
MDL 59	2304	2664	75	31.3	73.6	11.8	85.1	13.7
NGC 3557	3294	2957	60	38.7	85.0	14.4	76.3	12.9
NGC 0383	4924	5326	32	66.6	73.9	11.9	80.0	12.9
NGC 0507	4869	5257	99	57.3	84.9	13.5	91.8	14.6
Pavo 2	4398	4646	70	50.9	86.3	14.2	91.2	15.0
Pegasus	3545	3874	80	53.3	66.4	10.7	72.6	11.7
Ursa Major	1088	1088	40	19.8	54.8	8.6	54.8	8.6

TABLE 8

ADOPTED REVISED CEPHEID DISTANCES TO LEO I, VIRGO, AND FORNAX

Cluster/Group	μ_0 (mag)	$\pm\sigma$	D (Mpc)	$\pm\sigma$	μ_Z (mag)	$\pm\sigma$	D_Z (Mpc)
Leo I group[a]	29.90	0.10	9.5	0.4	30.01	0.09	10.0
Virgo Cluster[b]	30.81	0.04	14.6	0.3	30.92	0.05	15.3
Fornax Cluster[c]	31.32	0.17	18.3	1.4	31.39	0.20	19.0

[a] Based on distances to NGC 3351 and NGC 3368.
[b] Based on distances to NGC 4321, NGC 4496A, NGC 4535, NGC 4536, and NGC 4548.
[c] Based on distances to NGC 1326A, NGC 1365, and NGC 1425.

± 0.3 mag (Giovanelli et al. 1997; Sakai et al. 2000; Tully & Pierce 2000), or $\pm 15\%$ in distance for a single galaxy. In a broad sense, the Tully-Fisher relation can be understood in terms of the virial relation applied to rotationally supported disk galaxies, under the assumption of a constant mass-to-light ratio (Aaronson, Mould, & Huchra 1979). However, a detailed self-consistent physical picture that reproduces the Tully-Fisher relation (e.g., Steinmetz & Navarro 1999), and the role of dark matter in producing almost universal spiral galaxy rotation curves (McGaugh et al. 2000) still remain a challenge.

Macri et al. (2000) obtained new *BVRI* photometry, and using published data remeasured line widths for the Cepheid galaxies that are Tully-Fisher calibrators. Sakai et al. (2000) applied this calibration to a sample of 21 clusters out to 9000 km s^{-1} observed by Giovanelli et al. (1997), and to an *H*-band sample of 10 clusters from Aaronson et al. (1982, 1986). With an adopted distance to the LMC of 50 kpc, Sakai et al. determined a value of $H_0 = 71 \pm 4 \pm 7$ km s^{-1} Mpc^{-1}. Based on the same set of Key Project Cepheid calibrator distances, the same LMC zero point, and a compilation of *BRIK* data for Tully-Fisher cluster galaxies from the literature, Tully & Pierce (2000) determined a value of $H_0 = 77 \pm 8$ km s^{-1} Mpc^{-1} (at a quoted 95% confidence level). In the *I* band, where there is good overlap with Tully and Pierce, Sakai et al. found $H_0 = 73 \pm 2 \pm 9$ km s^{-1} Mpc^{-1}. Based on analyses using an earlier available subset of Cepheid calibrators, Giovanelli et al. (1997) concluded that $H_0 = 69 \pm 5$ km s^{-1} Mpc^{-1}, consistent with Madore et al. (1998), who obtained $H_0 = 72 \pm 5 \pm 7$ km s^{-1} Mpc^{-1}. However, for a consistent set of calibrators, the difference in these values probably reflects some of the systematic uncertainties inherent in implementing the Tully-Fisher technique. Tully & Pierce discuss at length possible reasons for the source of the differences among various published values of H_0 based on the Tully-Fisher relation, but they conclude that the reason for much of this discrepancy remains unresolved.

Adopting the same Tully-Fisher (*BVIH*) galaxy sample discussed in Sakai et al. (2000), applying the new PL calibration, and adopting the metallicity-corrected distances for the Tully-Fisher calibrators given in Table 4 results in a value of $H_0 = 71 \pm 3 \pm 7$ km s^{-1} Mpc^{-1}, with no net change from that published by Sakai et al. The adopted distances and velocities for the Tully-Fisher clusters used in this analysis are given in Table 7. Also tabulated are the velocities in the cosmic microwave background frame, and H_0 values and uncertainties.

6.3. *Fundamental Plane for Elliptical Galaxies*

For elliptical galaxies, a correlation exists between the stellar velocity dispersion and the intrinsic luminosity (Faber & Jackson 1976), analogous to the relation between rotation velocity and luminosity for spirals. Elliptical galaxies are found to occupy a "fundamental plane" ($r_e \propto \sigma^{\alpha}\langle I\rangle_e^{\beta}$) in which a defined galaxy effective radius (r_e) is tightly correlated with the surface brightness (I_e) within r_e, and central velocity dispersion of the galaxy (σ) (Dressler et al. 1987; Djorgovski & Davis 1987); and $\alpha \sim 1.2$ and $\beta \sim -0.85$ (Djorgovski & Davis 1987). The scatter in this relation is approximately 10%–20% in distance for an individual cluster.

Jorgensen, Franx, & Kjaergaard (1996) have measured the fundamental plane for 224 early-type galaxies in 11 clusters spanning $cz \sim 1000$–11,000 km s^{-1}. Kelson et al. (2000) provided a Cepheid calibration for the distant clusters

TABLE 9

FUNDAMENTAL PLANE HUBBLE CONSTANT

Cluster/Group	N	$V_{\rm CMB}$	$V_{\rm flow}$	D (Mpc)	σ	$H_0^{\rm CMB}$	σ	$H_0^{\rm flow}$	σ
Dorado	9	1131	1064	13.8	1.4	81.9	8.7	77.0	8.2
GRM 15	7	4530	4848	47.4	4.7	95.6	10.0	102.2	10.7
Hydra I	20	4061	3881	49.1	4.7	82.8	8.4	79.1	8.0
Abell S753	16	4351	3973	49.7	4.2	87.5	7.9	79.9	7.2
Abell 3574	7	4749	4617	51.6	5.3	92.0	10.0	89.5	9.7
Abell 194	25	5100	5208	55.9	4.3	91.3	7.5	93.2	7.6
Abell S639	12	6533	6577	59.6	5.1	109.7	9.9	110.4	10.0
Coma	81	7143	7392	85.8	5.9	83.2	6.0	86.1	6.2
Abell 539	25	8792	8648	102.0	7.4	86.2	6.5	84.7	6.4
DC 2345−28.....	30	8500	8708	102.1	7.4	83.2	6.4	85.2	6.5
Abell 3381	14	11536	11436	129.8	11.5	88.9	8.3	88.1	8.2

based on Key Project distances to spiral galaxies in the Leo I group, and the Virgo and Fornax Clusters, yielding $H_0 = 78 \pm 5 \pm 9$ km s^{-1} Mpc^{-1}. The revised Cepheid distances presented in this paper result in new distances to the Virgo Cluster, the Fornax Cluster, and the Leo I group (Table 8). The galaxies in these objects are among the most distant in the Key Project sample, and they also have high metallicities. Hence, the new calibration impacts the fundamental plane more than the other secondary methods analyzed here. The new calibration yields $H_0 = 82 \pm 6 \pm 9$ km s^{-1} Mpc^{-1}, adopting a metallicity correction of -0.2 ± 0.2 mag dex^{-1}. The number of galaxies, adopted distances, velocities, H_0 values, and uncertainties for the clusters in this analysis are given in Table 9.

6.4. *Surface Brightness Fluctuations*

Another method with high internal precision, developed by Tonry & Schneider (1988) and Tonry et al. (1997, 2000), makes use of the fact that the resolution of stars within galaxies is distance dependent. This method is applicable to elliptical galaxies or to spirals with prominent bulges. By normalizing to the mean total flux and correcting for an observed color dependence, relative distances to galaxies can be measured. The intrinsic scatter of this method is small: a factor of 3 improvement compared to the Tully-Fisher and D_n-σ relations makes the method an order of magnitude less susceptible to Malmquist biases. Application of the method requires careful removal of sources of noise, such as bad pixels on the detector or objects such as star clusters, dust lanes, background galaxies, and foreground stars. With *HST*, this method is now being extended to larger distances (Lauer et al. 1998); unfortunately, however, only six galaxies beyond the Fornax Cluster have published surface brightness fluctuation distances, with only four of them accurate enough to be of interest for cosmology. Furthermore, all lie within the very narrow range $cz = 3800$–5800 km s^{-1}, where local flow-field contributions to the observed velocities are still non-negligible ($\sim 15\%$ $v_{\rm CMB}$).

As part of the Key Project, Ferrarese et al. (2000a) applied an *HST* Cepheid calibration to the four Lauer et al. (1998) SBF galaxies, and derived $H_0 = 69 \pm 4 \pm 6$ km s^{-1} Mpc^{-1}. The results are unchanged if all six clusters are included. The largest sources of random uncertainty are the large-scale flow corrections to the velocities, combined with the very sparse sample of available galaxies. Most of the systematic uncertainty is dominated by the uncertainty in the Cepheid calibration of the method itself (Ferrarese et al. 2000a; Tonry et al. 2000). These three factors account for the 10% difference between the SBF-based values of H_0 derived by the KP and that of Tonry et al. (2000). Flow-corrected velocities, distances, and H_0 values for the six clusters with SBF measurements are given in Table 10. Applying our new calibration, we obtain $H_0 = 70 \pm 5 \pm 6$ km s^{-1} Mpc^{-1}, applying a metallicity correction of -0.2 mag dex^{-1}, as described in § 3.

6.5. *Type II Supernovae*

Type II supernovae result from massive stars. They are fainter, and show a wider variation in luminosity than the Type Ia supernovae. Although not "standard candles," Type II supernovae can yield distances through application of the Baade-Wesselink technique to their expanding atmospheres. By following the time evolution of spectra for the expanding atmosphere (yielding the radius as a function of time and velocity), in combination with the photometric angular size (yielding the ratio of the radius to the distance of the supernova), the distance to the supernova can be obtained. Recent applications of this technique have been undertaken by Schmidt, Eastman, & Kirschner (1994) and Eastman, Schmidt, & Kirschner (1996) using detailed model atmospheres to correct for the scattering in the atmosphere. In principle, the method can be applied independent of the local calibration of the extragalactic distance scale. The diversity of different methods is critical in constraining the overall systematic errors in the distances measured as part of the Key Project, since the underlying physics of expanding supernova atmospheres is completely independent of the Cepheid distance scale and its calibration. Based on 16 Type II supernovae, covering a range of redshifts from $cz = 1100$ to 14,600 km s^{-1}, Schmidt et al. (1994) determine a value of $H_0 = 73 \pm 6 \pm 7$ km s^{-1} Mpc^{-1}.

In Table 11, we list the three galaxies currently having both Cepheid and Type II supernovae (SN II) distances. The Type II supernovae distances are from Schmidt et al. (1994). The distances from the two methods agree well within the quoted errors, and a weighted fit for the three calibrators yields a mean difference in the distance moduli of 0.09 ± 0.14 mag, in the sense of the Cepheids giving slightly shorter distances. A fourth galaxy, NGC 3627, also has both a Cepheid and a Type II distance, but the latter has a quoted uncertainty of ± 1.00 mag. We did not include the observed SNe II for M81, M100, or NGC 1559 because Schmidt, Kirshner, & Eastman comment that these supernovae are peculiar SNe II. There are four galaxies in the Schmidt et al. (1994) sample having velocities in the range $\sim 2000 < v_{\rm CMB} < 14{,}000$. If we apply a Cepheid calibration based on the distances to the LMC, M101, and NGC 7331 to these distant SNe II, for which we adopt velocities corrected to the CMB frame, we find $H_0 = 72 \pm 9 \pm 7$ km s^{-1} Mpc^{-1}. This result does not change if the Cepheid distances are corrected for metallicity, since two of the calibrators (the LMC and M101) are not affected by the metallicity term, and the difference in distance modulus for NGC 7331 is only 0.03 mag. Hence, the value of H_0 remains unchanged after applying a metallicity correction to the Cepheid distances for SN II.

TABLE 10

SURFACE BRIGHTNESS FLUCTUATION HUBBLE CONSTANT

Galaxy	$V_{\rm flow}$	σ	D (Mpc)	σ	$H_0^{\rm flow}$	σ
NGC 4881.....	7441	300	102.3	24.8	72.7	18.7
NGC 4373.....	3118	508	36.3	3.8	85.9	17.2
NGC 0708.....	4831	300	68.2	6.7	70.8	8.6
NGC 5193.....	3468	551	51.5	4.2	67.3	12.4
IC 0429	3341	552	55.5	4.2	60.2	11.2
NGC 7014.....	5061	300	67.3	4.8	75.2	7.2

TABLE 11

COMPARISON OF NEARBY CEPHEID AND TYPE II SN DISTANCES

Supernova	Host	μ (Cepheid)	σ	μ (SN II)	σ
SN 1970G.....	M101	29.13	0.11	29.40	0.35
SN 1987A	LMC	18.50	0.10	18.50	0.13
SN 1989L	NGC 7331	30.84	0.09	31.20	0.51

We note that our results agree very well with Schmidt et al. (1994), despite the 5% difference in the distances seen in Table 11. However, we have limited our H_0 analysis to galaxies beyond $cz = 1500$ km s^{-1}, whereas 10 of the 14 galaxies in the Schmidt et al. sample are within this limit. The nearest supernovae (where flow field effects are largest) yield a higher value of H_0.

7. COMBINING THE RESULTS AND A VALUE FOR H_0

In Table 12, we list the values of H_0 obtained for each of the secondary methods that are based on our Cepheid distances, updated using the new calibration described in § 3.4. For each method, the formal random and systematic uncertainties are given. We defer until § 8 a detailed discussion of the systematic uncertainties that affect all of these methods equally; however, the dominant overall systematic errors include the uncertainty in the WFPC2 photometric calibration, and the uncertainty in the adopted distance to the LMC, metallicity, and bulk motions of galaxies on large scales ($cz \gtrsim 10{,}000$ km s^{-1}).

We next address the question of how to combine the values of H_0 obtained using the different secondary methods, given five independent measurements, H_i, with errors σ_i. All of these methods are based on a common Cepheid zero point, although with different subsets of Cepheid calibrators. We now treat the combination of these values using the quoted internal errors. The secondary methods themselves are largely independent of each other (for example, the kinematics of spiral disks represented by the Tully-Fisher relation are independent of the physics of the explosions of carbon-oxygen white dwarfs that give rise to Type Ia supernovae, and in turn are independent of the physics relating to the luminosity fluctuations of red giant stars used by SBF). We use three methods to combine the results: a classical (frequentist) analysis, a Bayesian analysis, and a weighting scheme based on numerical simulations. Because of the relatively small range of the individual determinations ($H_0 = 70$–82 km s^{-1} Mpc^{-1}, with most of the values clustered toward the low end of this range), all three methods for combining the H_0 values are in very good agreement. This result alone gives us confidence that the combined value is a robust one, and that the choice of statistical method does not determine the result, nor does it strongly depend on the choice of assumptions and priors.

In the Bayesian data analysis, a conditional probability distribution is calculated, based on a model or prior. With a Bayesian formalism, it is necessary to be concerned about the potential subjectivity of adopted priors and whether they influence the final result. However, one of the advantages of Bayesian techniques is that the assumptions about the distribution of probabilities are stated up front, whereas, in fact, all statistical methods have underlying but often less explicit assumptions, even the commonly applied frequentist approaches (including a simple weighted average, for example). A strong advantage of the Bayesian method is that it does not assume Gaussian distributions. Although more common, frequentist methods are perhaps not always the appropriate statistics to apply. However, the distinction is often one of nomenclature rather than subjectivity (Gelman et al. 1995; Press 1997).

In Figure 3, we plot probability distributions for the individual H_0 determinations (see Table 12), each represented by a Gaussian of unit area, with a dispersion given by their individual σ values. The cumulative distribution is shown by the solid thick line. The median value is $H_0 = 72 \pm 3$

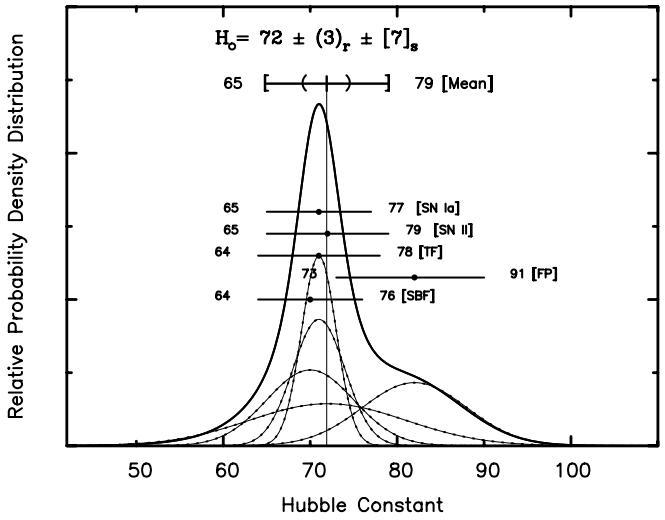

FIG. 3.—Frequentist probability density; values of H_0 and their uncertainties for Type Ia supernovae, the Tully-Fisher relation, the fundamental plane, surface brightness fluctuations, and Type II supernovae, all calibrated by Cepheid variables. Each value is represented by a Gaussian curve (*joined dots*) with unit area and a 1 σ scatter equal to the random uncertainty. The systematic uncertainties for each method are indicated by the horizontal bars near the peak of each Gaussian. The upper curve is obtained by summing the individual Gaussians. The cumulative (frequentist) distribution has a midpoint (median) value of $H_0 = 72(71) \pm 4 \pm 7$ km s^{-1} Mpc^{-1}. The overall systematic error is obtained by adding the individual systematic errors in quadrature.

TABLE 12

UNCERTAINTIES IN H_0 FOR SECONDARY METHODS

Method	H_0	Error (random, systematic) (%)	References
36 Type Ia SN, $4000 < cz < 30{,}000$ km s^{-1}	71	$\pm 2 \pm 6$	1, 2, 3, 4
21 TF clusters, $1000 < cz < 9000$ km s^{-1}	71	$\pm 3 \pm 7$	5, 6, 7
11 FP clusters, $1000 < cz < 11{,}000$ km s^{-1}	82	$\pm 6 \pm 9$	8, 9
SBF for 6 clusters, $3800 < cz < 5800$ km s^{-1}	70	$\pm 5 \pm 6$	10, 11
4 Type II SN, $1900 < cz < 14{,}200$ km s^{-1}	72	$\pm 9 \pm 7$	12

NOTE—Combined values of H_0: $H_0 = 72 \pm 2$ (random) km s^{-1} Mpc^{-1} (Bayesian), $H_0 = 72 \pm 3$ (random) km s^{-1} Mpc^{-1} (frequentist); $H_0 = 72 \pm 3$ (random) km s^{-1} Mpc^{-1} (Monte Carlo)

REFERENCES.—(1) Hamuy et al. 1996; (2) Riess et al. 1998; (3) Jha et al. 1999; (4) Gibson et al. 2000a; (5) Giovanelli et al. 1997; (6) Aaronson et al. 1982, 1986; (7) Sakai et al. 2000; (8) Jorgensen et al. 1996; (9) Kelson et al. 2000; (10) Lauer et al. 1998; (11) Ferrarese et al. 2000a; (12) Schmidt et al. 1994.

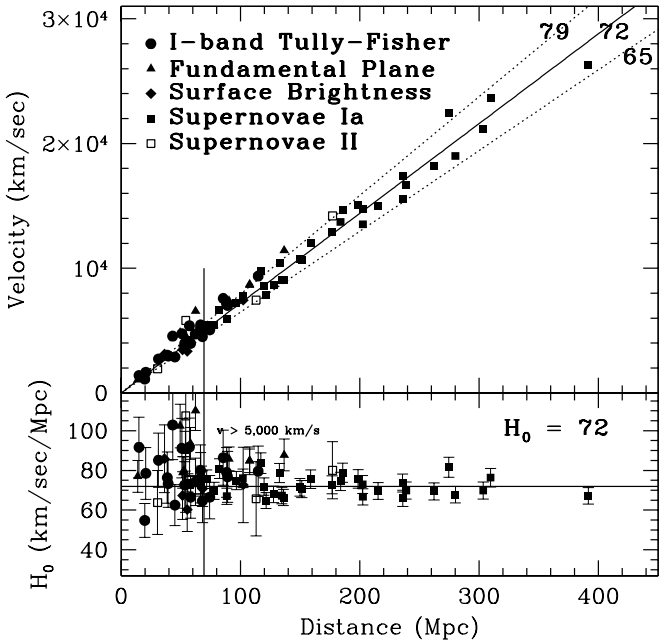

FIG. 4.—*Top*: Hubble diagram of distance vs. velocity for secondary distance indicators calibrated by Cepheids. Velocities in this plot are corrected for the nearby flow model of Mould et al. (2000a). *Squares*: Type Ia supernovae; *filled circles*: Tully-Fisher clusters (*I*-band observations); *triangles*: fundamental plane clusters; *diamonds*: surface brightness fluctuation galaxies; *open squares*: Type II supernovae. A slope of $H_0 = 72$ is shown, flanked by $\pm 10\%$ lines. Beyond 5000 km s^{-1} (*vertical line*), both numerical simulations and observations suggest that the effects of peculiar motions are small. The Type Ia supernovae extend to about 30,000 km s^{-1}, and the Tully-Fisher and fundamental plane clusters extend to velocities of about 9000 and 15,000 km s^{-1}, respectively. However, the current limit for surface brightness fluctuations is about 5000 km s^{-1}. *Bottom*: Value of H_0 as a function of distance.

± 7 km s^{-1} Mpc^{-1}. The random uncertainty is defined at the $\pm 34\%$ points of the cumulative distribution. The systematic uncertainty is discussed below. For our Bayesian analysis, we assume that the priors on H_0 and on the probability of any single measurement being correct are uniform and compute the project of the probability distributions. In this case, we find $H_0 = 72 \pm 2 \pm 7$ km s^{-1} Mpc^{-1}. The formal uncertainty on this result is very small, and simply reflects the fact that four of the values are clustered very closely, while the uncertainties in the FP method are large. Adjusting for the differences in calibration, these results are also in excellent agreement with the weighting based on numerical simulations of the errors by Mould et al. (2000a), which yielded 71 ± 6 km s^{-1} Mpc^{-1}, similar to an earlier frequentist and Bayesian analysis of Key Project data (Madore et al. 1999) giving $H_0 = 72 \pm 5 \pm 7$ km s^{-1} Mpc^{-1}, based on a smaller subset of available Cepheid calibrators.

As is evident from Figure 3, the value of H_0 based on the fundamental plane is an outlier. However, both the random and systematic errors for this method are larger than for the other methods, and hence the contribution to the combined value of H_0 is relatively low, whether the results are weighted by the random or systematic errors. We recall also from Table 1 and § 6 that the calibration of the fundamental plane currently rests on the distances to only three clusters. If we weight the fundamental-plane results factoring in the small number of calibrators and the observed variance of this method, then the fundamental plane has a weight that ranges from 5 to 8 times smaller than any of the other four methods, and results in a combined, metallicity-corrected value for H_0 of 71 ± 4 (random) km s^{-1} Mpc^{-1}.

Figure 4 displays the results graphically in a composite Hubble diagram of velocity versus distance for Type Ia supernovae (*filled squares*), the Tully-Fisher relation (*filled circles*), surface-brightness fluctuations (*filled diamonds*), the fundamental plane (*filled triangles*), and Type II supernovae (*open squares*). In the bottom panel, the values of H_0 are shown as a function of distance. The Cepheid distances have been corrected for metallicity, as given in Table 4. The Hubble line plotted in this figure has a slope of 72 km s^{-1} Mpc^{-1}, and the adopted distance to the LMC is taken to be 50 kpc.

8. OVERALL SYSTEMATIC UNCERTAINTIES

There are a number of systematic uncertainties that affect the determination of H_0 for all the relative distance indicators discussed in the previous sections. These errors differ from the statistical and systematic errors associated with each of the individual secondary methods, and they cannot be reduced by simply combining the results from different methods. Significant sources of overall systematic error include the uncertainty in the zero point of the Cepheid PL relation, the effect of reddening and metallicity on the observed PL relations, the effects of incompleteness bias and crowding on the Cepheid distances, and velocity perturbations about the Hubble flow on scales comparable to, or larger than, the volumes being sampled. Since the overall accuracy in the determination of H_0 is constrained by these factors, we discuss each one of these effects in turn below. For readers who may wish to skip the details of this part of the discussion, we refer them directly to § 8.7 for a summary.

8.1. *Zero Point of the PL Relation*

It has become standard for extragalactic Cepheid distance determinations to use the slopes of the LMC period-luminosity relations as fiducial, with the zero point of the Cepheid period-luminosity relation tied to the LMC at an adopted distance modulus of 18.50 mag (e.g., Freedman 1988). However, over the past decade, even with more accurate and sensitive detectors, with many new methods for measuring distances, and with many individuals involved in this effort, the full range of the most of distance moduli to the LMC remains at approximately 18.1–18.7 mag (e.g., Westerlund 1997; Walker 1999; Freedman 2000a; Gibson 2000), corresponding to a range of 42–55 kpc.

For the purposes of the present discussion, we can compare our adopted LMC zero point with other published values. We show in Figure 5 published LMC distance moduli expressed as probability density distributions, primarily for the period 1998–1999, as compiled by Gibson (2000). Only the single most recent revision from a given author and method is plotted. Each determination is represented by a Gaussian of unit area, with dispersions given by the published errors. To facilitate viewing the individual distributions (Fig. 5, *light dotted lines*), these have been scaled up by a factor of 3. The thicker solid line shows the cumulative distribution.

It is clear from the wide range of moduli compared to the quoted internal errors in Figure 5 that systematic errors affecting individual methods are still dominating the determinations of LMC distances. Some of the values at either end of the distribution have error bars that do not overlap

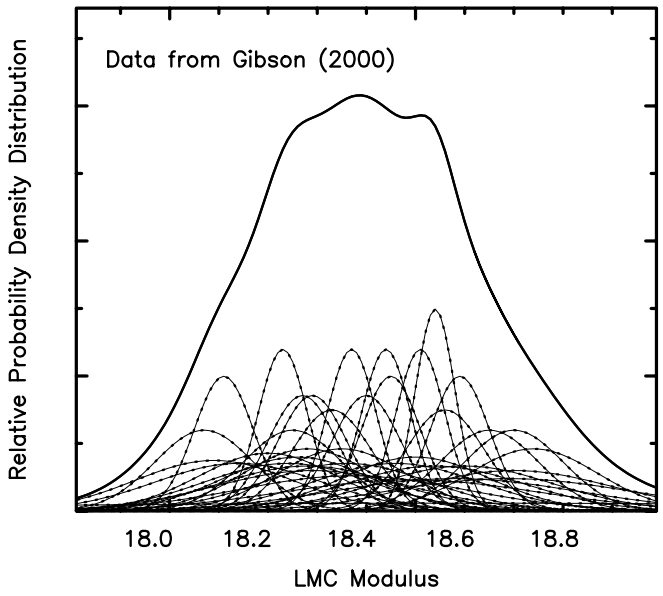

FIG. 5.—Frequentist probability density; distribution of LMC distance moduli as compiled by Gibson (2000) plotted as a continuous probability density distribution built up from the sum of individual unit-area Gaussians centered at the quoted modulus, and broadened by the published internal random error.

(at several σ) with other methods. At present, there is no single method with demonstrably lower systematic errors, and we find no strong reason to prefer one end of the distribution over the other. For example, while systematics in the Cepheid period-luminosity relation have been subjected to scrutiny for many decades, no accurate photometric zero point has yet been established based on astrometric distances, and the zero point is still in debate (e.g., Feast & Catchpole 1997; Madore & Freedman 1998; Groenewegen & Oudmaijer 2000). The absolute astrometric calibration is statistically more reliable for the red clump method, but compared to many other methods, this method is still relatively new, and the systematics have not been studied in as much detail (Udalski 2000; Stanek et al. 2000).

In addition to the cumulative probability distributions, we have computed Bayesian probability distributions, assuming a uniform prior. The Bayesian and median or average frequentist methods yield excellent agreement at 18.45 and 18.47 mag, respectively. Another way of estimating the overall uncertainty is simply to estimate the overall average and the standard error of the mean, based on a mean distance for different methods, and giving each technique unit weight. An advantage of this procedure is that it simply averages over all the inherent systematic uncertainties that affect any given method. There are seven independent methods for measuring distances that are commonly applied to the LMC; these include Cepheids, the red clump, eclipsing binaries, SN 1987A light echoes, tip of the red giant branch (TRGB), RR Lyrae stars, and Mira variables. The mean values of the LMC distance moduli and the standard error of the mean for each technique are given in Table 13, for the Gibson (2000) and Westerlund (1997) compilations. For the Gibson compilation, these averaged distance moduli range from 18.27 to 18.64 mag, with an overall mean of 18.45 mag, and an rms dispersion of ± 0.15 mag. The standard error of the mean therefore amounts to ± 0.06 mag. The mean based on the Westerlund data is in excellent agreement at 18.46 ± 0.05 mag.

From the above discussion, it can be seen that there still remains a range in distance moduli to the LMC based on a wide range of methods. However, our adopted Cepheid modulus of 18.50 ± 0.10 mag agrees with the mean and median of the distribution for other methods at the 2.5% level.[22] Given the remaining uncertainties and the good agreement with other methods, we do not believe that a change in zero point is warranted at present. However, we note that the uncertainty in the distance to the LMC is one of the largest remaining uncertainties in the overall error budget for the determination of H_0. We note that if the distance modulus to the LMC is 18.3 mag, there will be a resulting 10% increase in the value of H_0 to 79 km s^{-1} Mpc^{-1}.

It would be extremely useful to have a calibration that is independent of the distance to the LMC. Very recently, a new distance has been independently measured to the maser galaxy NGC 4258, a nearby spiral galaxy also useful for calibrating the extragalactic distance scale, which can provide an external check on the adopted LMC zero-point calibration. We briefly summarize the distance determination to NGC 4258 and its implications below.

8.1.1. *NGC 4258: Comparison of a Maser and Cepheid Distance*

Given the current uncertainties and systematics affecting the local distance scale, it would be highly desirable to have geometric methods for measuring distances, independent of

[22] In two recent Key Project papers, we adopted a distance modulus uncertainty to the LMC of ± 0.13 mag (Mould et al. 2000a; Freedman 2000b). This value defined the 1 σ dispersion based on a histogram of the distance moduli compiled by Gibson (2000). However, the standard error of the mean is the relevant statistic in this case.

TABLE 13

LMC DISTANCE MODULI FOR DIFFERENT METHODS

Method	$\langle \mu_0 \rangle$[a] (mag)	σ (mag)	N	$\langle \mu_0 \rangle$[b] (mag)	σ (mag)	N
Cepheids	18.57	± 0.14	5	18.52	± 0.13	15
Eclipsing variables	18.33	± 0.05	3	...	...	...
SN 1987A	18.47	± 0.08	4	18.50	± 0.12	5
TRGB	18.64	± 0.05	2	18.42	± 0.15	1
Red clump	18.27	± 0.11	10	...	...	...
RR Lyrae variables	18.30	± 0.13	7	18.40	± 0.19	14
Mira variables	18.54	± 0.04	3	18.46	± 0.11	4

[a] Based on Gibson 2000 compilation.
[b] Based on Westerlund 1997 compilation.

the classical distance indicators. A very promising new geometric technique has recently been developed and applied to the galaxy NGC 4258, a galaxy with an inner disk containing H_2O masers (Herrnstein et al. 1999). Five epochs of measurements are now available for these masers, and both radial and transverse motions of the maser system have been measured. Assuming a circular Keplerian model for the disk, Herrnstein et al. derive a distance to the galaxy of 7.2 ± 0.3 Mpc, with the error increasing to ± 0.5 Mpc allowing for systematic uncertainties in the model.

To provide a comparison with the maser distance, Maoz et al. (1999) used *HST* to discover a sample of 15 Cepheids in NGC 4258. Adopting a distance modulus for the LMC of 18.50 mag, these authors determined a Cepheid distance to NGC 4258 of 8.1 ± 0.4 Mpc, or 12% farther than the maser distance. These authors noted that the difference was not highly significant, amounting to only 1.3 σ. However, with the new LMC PL relations given in equations (1) and (2) and the correction to the WFPC2 zero point discussed in § 2.5, the revised Cepheid distance is in somewhat better agreement with the maser distance at $7.8 \pm 0.3 \pm 0.5$ Mpc (Newman et al. 2000).[23] This distance allows for a metallicity correction of -0.2 mag dex^{-1}. Unfortunately, however, the situation remains that there is currently only one maser galaxy with which to make this comparison. For the future, increasing the sample of maser galaxies for which distance measurements can be made (for example, with *ARISE*, a proposed radio interferometer in space) would be extremely valuable.

8.1.2. *Resolving the Cepheid Zero-Point Discrepancy*

Given the range of published LMC distance moduli (Fig. 5) and the subtle systematic errors that must be affecting some (or all) of the distance methods, it appears unlikely that this zero-point uncertainty will be resolved definitively any time soon. Upcoming interferometry (NASA's *SIM* and ESA's *GAIA*) missions will deliver a few microarcsecond astrometry, reaching fainter limits than *Hipparcos* (~ 20 mag); NASA's *FAME* will reach 50 mas accuracy. These missions are capable of delivering 1% distances to many Galactic Cepheids. They will be critical for establishing a more accurate extragalactic distance scale zero point, and should provide accurate parallaxes for statistically significant samples of many distance indicators currently in use (e.g., Cepheids, RR Lyrae stars, red giant stars, red clump stars). In addition, *SIM* (currently scheduled for launch in 2008) may provide rotational parallaxes for some of the nearest spiral galaxies, thereby allowing the calibration to bypass the LMC altogether.

8.2. *Reddening*

As described in § 3.1, the standard approach to correcting Cepheid magnitudes for reddening by dust is to use a combination of bandpasses (V and I in the case of the H_0 Key Project), and solve for the reddening using a Galactic extinction law (Freedman 1988). For a value of the LMC reddening appropriate to the Cepheid sample considered of $E(V-I) = 0.13$ mag, the reddenings in the *HST* Cepheid target fields range from $E(V-I) = 0.04$ to 0.36 mag, with an average of 0.19 mag (Table 4). As a check on possible systematic errors in the reddening determinations, recent H-band (1.6 μm) photometry has been obtained for a total sample of 70 Cepheids in 12 galaxies, including IC 1613, M31, M81, M101, NGC 925, NGC 1365, NGC 2090, NGC 3198, NGC 3621, NGC 4496A, NGC 4536, and IC 4182 (Macri et al. 2001; W. L. Freedman et al., in preparation). The Galactic reddening law of Cardelli et al. (1989) predicts $E(V-H) = 1.98 \pm 0.16\, E(V-I)$. For the galaxies with both NICMOS H-band and optical VI data (from the ground or *HST*), the slope of the correlation between the optical and near-infrared reddenings yields $E(V-H) = [2.00 \pm 0.22\, E(V-I)] + 0.02 \pm 0.04$. This relation is based on the same VI Udalski et al. (1999) data used in the current paper. Hence, the IR data confirm the reddenings derived from the optical data alone, ruling out a significant systematic error in the reddening determinations.

8.3. *Metallicity*

As discussed in § 3.2, recent empirical results suggest that there is a small dependence of the Cepheid period-luminosity relation on metallicity. In this paper, we have adopted a correction of -0.2 mag (10% in distance) for a factor of 10 in abundance (O/H). The observed fields in Cepheid-calibrating galaxies have a range in (O/H) abundance of about a factor of 30 (Ferrarese et al. 2000b). These abundances are those of H II regions in the Cepheid fields, calibrated on the scale of Zaritsky, Kennicutt, & Huchra (1994). The mean abundance of this sample [$12 + \log$ (O/H)] is 8.84 ± 0.31 dex. This is higher than the LMC abundance of 8.50 dex (Kennicutt et al. 1998). The mean offset between the metallicity-corrected and the uncorrected Cepheid moduli in Table 4 amounts to 0.07 mag, or 3.5% in distance. We adopt this difference as the uncertainty due to metallicity. The effect is systematic, and with the exception of Type II supernovae (§ 6.5), if no correction for metallicity is applied, the value of H_0 is increased by $\sim 4\%$ (~ 3 km s^{-1} Mpc^{-1}). Conversely, if the slope of the metallicity relation is -0.4 mag dex^{-1}, then the value of H_0 is decreased by 3 km s^{-1} Mpc^{-1}. We show in Figure 6 histograms of abundance distributions for the Cepheid calibrators for the secondary methods.

8.4. *Completeness and Bias Effects*

An issue of recurring concern regarding the application of distance indicators is the extent to which incompleteness in the observed samples could lead to a bias in the derived distances. This effect has been discussed extensively in the literature, particularly in the context of the Tully-Fisher relation (e.g., Schechter 1980; Willick 1994; Giovanelli et al. 1997; Tully & Pierce 2000). For Cepheids, the concern derives from the fact that magnitude cutoffs in the Cepheid samples (imposed by the decreasing signal-to-noise ratios at faint magnitudes) will tend to select against the faintest variables, thereby leading to systematically small (biased) moduli. The fact that the bias operates most strongly at the shortest periods will also tend to produce a flattening of the observed PL relation (see, e.g., Sandage 1988); elimination of the shortest period Cepheids from a sample will generally result in increased mean moduli, less affected by this bias.

This effect is illustrated in Figure 10 in the Appendix, along with an analytic derivation of the size of the bias. As more distant objects are observed, a brighter intrinsic magnitude cutoff will occur for the same apparent magnitude. The observed erroneous flattening of the PL slope extends

[23] The distances presented in the current paper are for ALLFRAME magnitudes Tables 3 and 4; note that the new ALLFRAME distance to NGC 4258 is 8.0 Mpc, in slightly worse disagreement with the maser distance that that given in Newman et al. and quoted above.

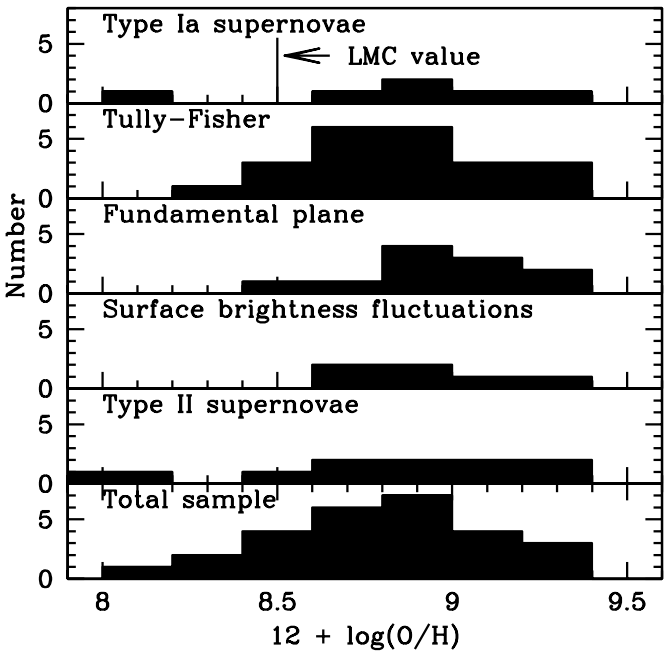

FIG. 6.—Histograms for the distributions of oxygen abundances [12 + log (O/H)] from Ferrarese et al. (2000b) for the galaxies with Cepheid distances that calibrate Type Ia supernovae, the Tully-Fisher relation, the fundamental plane, surface brightness fluctuations, and Type IIa supernovae. The metallicity of the LMC in these units is 8.50 dex. The total distribution is also shown. In the mean, most of the Cepheid fields observed have higher abundances than the LMC.

to longer and longer periods, including more and more of the available Cepheid sample. Similar biases occur for any standard candle possessing an intrinsic dispersion in luminosity: the larger the intrinsic dispersion of the relation being truncated, and the shallower the range of apparent magnitude being sampled, the larger the bias will be. For the Key Project application of the Tully-Fisher relation (Sakai et al. 2000), we adopted corrections for this incompleteness bias, based on simulations similar to those undertaken by Giovanelli et al. (1998). For Type Ia supernovae, the observed dispersion in the Hubble diagram amounts to only $\sim$0.15 mag (e.g., Riess et al. 1998; Hamuy et al. 1996); hence, incompleteness biases are very small for this technique.

In the case of Cepheids, incompleteness biases are expected to be small for the methodology that we have adopted here. First, the intrinsic scatter is small, and second, as discussed in § 3.4, we have applied a period cutoff above the limiting magnitude cutoff at the short-period end to reduce the incompleteness bias (Freedman et al. 1994b; Kelson et al. 1996; Ferrarese et al. 1996, 2000b). The scatter in the observed V-band PL relation amounts to $\pm$0.16 mag (eq. [1]); the scatter in the I-band PL relation amounts to $\pm$0.11 mag (eq. [2]); however, much of this scatter is physically correlated between bandpasses, so that the scatter in the W PL relation is small. After correcting for reddening, the correlated scatter in the combined relation for the true distance modulus (or equivalently, W; see § 3.1) is smaller, and amounts to only $\pm$0.08 mag (eq. [3]). Hence, the resulting bias on the final distance modulus is negligible for most of the galaxies in the sample. As can be seen from the differences between columns (5) and (7) in Table 3, typically the size of the bias corrections amounts to only a few hundredths of a mag in the reddening-corrected (true) modulus; in two cases (M81 and NGC 4414) they are as large as 0.08 and $-$0.08 mag (4% in distance), respectively, but the mean correction for the sample is only $+$0.01 mag.

8.5. *Crowding and Artificial Star Tests*

One of the most direct ways of assessing the quantitative effects of chance superpositions on the photometry is by adding artificial stars with known input magnitudes and colors into the actual *HST* images, and then recovering those stars using exactly the same techniques used to perform the original analysis (i.e., ALLFRAME and DoPHOT). While these experiments cannot provide numerical crowding corrections to the real Cepheids in the frames, they are powerful in quantifying the vulnerability of the photometric methods to crowding under each individual set of circumstances.

Artificial star tests for two Key Project galaxies have been carried out by Ferrarese et al. (2000c). Their analysis indicates that the bias due to crowding in individual WFPC2 frames can be significant, ranging from 0.05 mag in a relatively uncrowded field of NGC 2541 (at 12 Mpc) to 0.2 mag for a crowded field in one of the most distant galaxies, NGC 1365. We note that the artificial stars in these frames were not inserted with random positions. Each field was divided up into a 10 $\times$ 10 array of cells each 65 pixels on a side; the probability that an artificial star would be added within a given cell was therefore proportional to the number of real stars in the cell. The measured bias goes in the expected sense of resulting in recovered magnitudes that are too bright, and it is a direct function of the stellar density in the field. However, when using the multiepoch V- and I-band observations, and then imposing the same criteria on variable star selection as for the actual Cepheid sample (e.g., same error flags for deviant data points, same magnitude range applicable to the period range for the known Cepheids, the same procedure for reddening correction, etc.), the effect of this bias on the final determination of distances drops significantly, amounting to only 1% for ALLFRAME, and 2% for DoPHOT.

The Ferrarese et al. (2000c) results are consistent with an independent study by Saha et al. (2000), who have investigated the effects of crowding in the galaxy NGC 4639 (at a distance of $\sim$25 Mpc, the largest distance measured by either the Key Project or Type Ia supernova teams). For this galaxy, the crowding bias in single-epoch observations is found to be 4% (0.07 mag). Saha et al. do not explicitly extend their results to observations of Cepheids at multiple epochs, for which, as noted above, the effect would be reduced even further. A different approach to placing limits on crowding effects comes from Gibson et al. (2000b) and Ferrarese et al. (2000c), who have looked for a correlation with distance of residuals in the Tully-Fisher relation. No significant effect is found. Gibson et al. also see no such systematic effects as would be expected for Type Ia supernova peak magnitudes, nor a difference in the PC- versus WFC-based Cepheid distance moduli.

Very different conclusions have recently been reached by Stanek & Udalski (1999) and Mochesjska (2000). These authors have specifically investigated the influence of blending on the Cepheid distance scale. Blending is the close association of a Cepheid with one or more intrinsically luminous stars. Since Cepheids are young stars, they may be preferentially associated near other young stars. Stanek & Udalski conclude that this effect ranges from a few percent

for nearby galaxies to ~15%–20% for galaxies at 25 Mpc. However, the Stanek & Udalski results are based on an extrapolation from high surface brightness regions in the bar of the LMC, and they do not make use of photometric reduction programs (such as DoPHOT and ALLFRAME), which are designed for photometry in crowded fields. These authors simply sum additional contributions to the total flux to simulate crowding. Moreover, they do not allow for underlying background contamination, which becomes increasingly important for galaxies at larger distances. Hence, at present, it is not possible to compare these results directly to the analysis of H_0 Key Project data.

In a comparison of ground-based images of M31 with *HST* images, Mochejska et al. (2000) found that the median V-band flux contribution from luminous companions was about 12% of the flux of the Cepheid. They argued that ground-based resolution in M31 corresponds to *HST* resolution at about 10 Mpc, and that blending will lead to systematically low distances for galaxies at such distances. A more recent study by this group for the galaxy M33, which has a much larger sample of stars, indicates that this effect amounts to only about 7% (Mochejska et al. 2001).

The exact size of this effect will depend on the true underlying distribution of stars in the frame, and the extent to which the actual Cepheids being measured are affected. We note that the galaxies with *HST* Cepheid distances for which blending effects are likely to be most severe are the inner field of M101, the high surface brightness galaxy NGC 3627, and the most distant galaxies searched, for example NGC 4639.

To assess quantitatively the impact of unresolved blending effects on the final Cepheid distances would require simulations based on the distribution of Cepheids in a galaxy field unaffected by blending. This distribution could be scaled with distance and inserted at the same surface brightness levels encountered in each of the Cepheid target frames, and then recovered using the same techniques as used originally to analyze the original data frames. Ideally, several input distributions could be tested. Such a study is beyond the scope of the present paper, but has been applied, for example, to the Cepheids observed in M101 with NICMOS (Macri et al. 2001).

Naive tests, which, for example, assume constant surface brightness between the Cepheid fields in nearby and distant galaxies, will not, in general, correctly simulate the Key Project, for which generally low surface brightness fields were deliberately selected. Examination of the statistics of the number densities of stars in the vicinity of Cepheids in the Key Project frames bear this out. For the present, we view the 2% effect measured by Ferrarese et al. (2000c) as a lower limit on the effects of crowding and blending, and adopt a conservative uncertainty of $+5\%$, -0% ($1\ \sigma$).

8.5.1. *Contamination from Companion Stars*

We note that Cepheids can be located in binary systems, and the presence of *true, physical companions* has been established for Cepheids in both the Galaxy and the LMC. For Cepheids in the Galaxy, as well as for early (B-type) stars, the mass distribution of companions has been studied intensively, and is strongly peaked toward low masses (e.g., Evans 1995). The presence of binaries will add increased scatter to the underlying period-luminosity relation, including that for the LMC, where the binaries are unresolved. However, unless the frequency of Cepheid binaries varies significantly from galaxy to galaxy, the relative distances to galaxies will be unaffected.

8.6. *Does the Measured Value of H_0 Reflect the True, Global Value?*

Locally, variations in the expansion rate due to large-scale velocities make measurement of the true value of H_0 problematic. Thus, for an accurate determination of H_0, a large enough volume must be observed to provide a fair sample of the universe over which to average. How large is large enough? Both theory and observations can provide constraints.

A number of theoretical studies have addressed this question recently. Given a model for structure formation, and therefore a predicted power spectrum for density fluctuations, local measurements of H_0 can be compared with the global value of H_0 (Turner, Cen, & Ostriker 1992; Shi & Turner 1998; Wang, Spergel, & Turner 1998). Many variations of cold dark matter (CDM) models have been investigated, and issues of both the required volume and sample size for the distance indicator have been addressed. The most recent models predict that variations at the level of 1%–2% in $\langle(\delta H/H_0)^2\rangle^{1/2}$ are to be expected for the current (small) samples of Type Ia supernovae that probe out to 40,000 km s^{-1}, whereas for methods that extend only to 10,000 km s^{-1}, for small samples, the cosmic variation is predicted to be 2%–4%.

There are also observational constraints that can test the possibility that we live in an underdense region locally. These include the observational determinations that the expansion is linear on 100–1000 Mpc scales, and measurements of temperature fluctuations in the cosmic microwave background. The linearity of the Hubble diagram has been established by many means, including work by Sandage & Hardy (1973) and Lauer & Postman (1992) on brightest cluster galaxies, recent studies of supernovae at velocity distances out to 30,000 km s^{-1} (Zehavi et al. 1998), and extension of the Tully Fisher relation to 15,000 km s^{-1} (Giovanelli et al. 1999; Dale et al. 1999). These results limit the difference between the global and local values of the Hubble constant to a few percent. For example, Giovanelli et al. provide limits to the amplitude of a possible distortion in the Hubble flow within 70 h^{-1} Mpc of $\delta H/H = 0.010 \pm 0.022$. The rarity of low-density bubbles is also attested by the microwave dipole anisotropy on degree scales. Wang et al. (1998) find a robust upper limit on the global deviation from the local 10^4 km s^{-1} sphere of 10.5% in H_0 with 95% confidence.

A stronger constraint will come from galaxy counts in redshift shells. If the local density were deficient within 150 Mpc by $\delta n/n = \delta\rho/\rho \lesssim -0.2$, the effect on H_0 would be

$$\frac{\delta H}{H} = \frac{1}{3}\,\Omega_m^{0.6}\,\frac{\delta\rho}{\rho}\,.$$

For example, for $\Omega_m = 0.2$, this is consistent with $1.0 > H(\text{global})/H(\text{local}) \gtrsim 0.97$. These results limit the difference between the global and local values of the Hubble constant to a few percent. This is consistent with the results cited above. [For comparison, with $\Omega_m = 1$, it is consistent with $1.0 > H(\text{global})/H(\text{local}) \gtrsim 0.93$.]

There are two sources of data on $\delta n/n$. The slope of galaxy counts versus magnitude is a relatively weak constraint, since excellent knowledge of the luminosity function of galaxies is required in order to infer a density. Redshift

survey data are superior; however, selection effects must be well understood before $\delta n/n$ can be determined. Improved constraints will soon be forthcoming from the Two-Degree Field (2dF), Sloan, 2 Micron All-Sky (2MASS), and 6dF surveys.

The overall conclusion derived from these studies is that uncertainties due to inhomogeneities in the galaxy distribution likely affect determinations of H_0 only at the few percent level. This must be reflected in the total uncertainty in H_0; however, the current distance indicators are now being applied to sufficiently large depths, and in many independent directions, that large errors due to this source of uncertainty are statistically unlikely. These constraints will tighten in the near future as larger numbers of supernovae are discovered, when all-sky measurements of the CMB anisotropies are made at smaller angular scales, and when deeper redshift surveys have been completed.

8.7. *Overall Assessment of Systematic Uncertainties*

We now briefly summarize the sources of systematic error discussed in the previous section. The standard error of the mean for the zero point of the LMC PL relation is ± 0.06 mag, and is currently set by an average over several independent methods. Conservatively, we adopt a value of ± 0.1 mag, corresponding to $\pm 5\%$ in the uncertainty for the distance to the LMC. Systematic errors in the reddening determinations are small, amounting to less than 1%. Both observational and theoretical studies of Cepheids suggest that there is a small metallicity dependence of the PL relation. Cepheid galaxies have a range of metallicities that are in the mean a few tenths of a dex greater that of the LMC. Adopting a metallicity correction results in values of H_0 that are lower in the mean by 4%. We take this difference between corrected and uncorrected distances to be indicative of the uncertainty due to metallicity. Cepheid distances can be affected by incompleteness biases at the few percent level, but these are minimized by adopting a conservative choice for the lower period limit, and by the fact that the dispersion in the reddening-corrected PL relation is only ± 0.08 mag. Ultimately, this sample bias effect contributes less than $\pm 1\%$ uncertainty to the final results. Based on artificial star experiments, crowding effects on the final distances also contribute at a 1%–2% level. Allowing for unresolved blending effects, we adopt an overall uncertainty of $+5\%, -0\%$. Finally, based on a number of both empirical and theoretical studies, bulk motions on very large scales are likely to contribute less than $\pm 5\%$.

Correcting for the effects of bias and metallicity decrease H_0 by 1% and 4%, respectively, whereas the effect of the new WFPC2 zero point is to increase H_0 by 3.5%. The effect of adopting the new Udalski et al. (1999) PL slopes differs from galaxy to galaxy (and therefore differs in the magnitude of the effect on the zero point for each secondary method). Adopting the new slopes results in a mean decrease in distance from the Madore & Freedman (1991) calibration of 7% for the galaxies listed in Table 3, but each individual method is impacted slightly differently depending on what subset of calibrators is applicable to that method. The sign of the uncertainty due to a possible bulk-flow component to the velocity field is, of course, unknown. In this paper, we have not applied a correction for crowding, but incorporate this uncertainty into the final error budget. These corrections individually amount to a few percent, but with differing signs so that the overall impact on the mean value of the Hubble constant agree at the 1% level with those in Mould et al. (2000a) and Freedman (2000b).

We list the major identified systematic uncertainties in Table 14; these can be combined in quadrature to yield an overall systematic uncertainty of $\pm 10\%$ (or 7 km s^{-1} Mpc^{-1}). Our current H_0 value incorporates four refinements discussed in detail above: (1) adopting the slopes of the PL relations as given by Udalski et al. (1999), (2) using the WFPC2 photometric zero-point calibration of Stetson (1998), (3) applying a metallicity correction of -0.2 ± 0.2 mag dex^{-1}, and (4) correcting for bias in the PL relation. Applying the resulting Cepheid calibration to five secondary methods gives $H_0 = 72 \pm 3 \pm 7$ km s^{-1} Mpc^{-1}.

9. H_0 FROM METHODS INDEPENDENT OF CEPHEIDS

A detailed discussion of other methods is beyond the scope of this paper; however, we briefly compare our results with two other methods: the Sunyaev-Zeldovich (SZ) technique, and measurement of time delays for gravitational lenses. Both of these methods are entirely independent of the local extragalactic distance scale, and they can be applied directly at large distances. Currently their accuracies are not yet as high as has recently been achieved for the classical distance measurements, but both methods hold considerable promise for the future. We show in Figure 7 values of H_0 published based on these two methods from 1991 to the present.

9.1. *The Sunyaev-Zeldovich Effect*

For clusters of galaxies, the combination of a measurement of the microwave background decrement (the Sunyaev-Zeldovich or SZ effect), the X-ray flux, and an assumption of spherical symmetry yield a measurement of

TABLE 14

OVERALL SYSTEMATIC ERRORS AFFECTING ALL METHODS

Source of Uncertainty	Description	Error (%)
LMC zero point	Error on mean from Cepheids, TRGB, SN 1987A, red clump, eclipsing binaries	± 5
WFPC2 zero point	Tie-in to Galactic star clusters	± 3.5
Reddening	Limits from NICMOS photometry	± 1
Metallicity	Optical, NICMOS, theoretical constraints	± 4
Bias in Cepheid PL	Short-end period cutoff	± 1
Crowding	Artificial star experiments	$+5, -0$
Bulk flows on scales >10,000 km s^{-1}	Limits from SN Ia, CMB	± 5

NOTE.—Adopted final value of H_0: $H_0 = 72 \pm 3$ (random) ± 7 (systematic) km s^{-1} Mpc^{-1}.

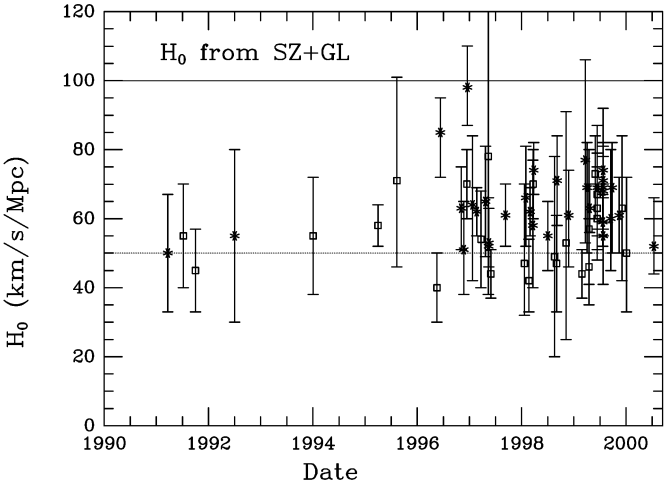

FIG. 7.—Values of the Hubble constant determined using the Sunyaev-Zeldovich effect (*open squares*) and gravitational lens time delays (*asterisks*) from 1990 to the present. From the compilation of Huchra (http://cfa-www.harvard.edu/~huchra) for the Key Project.

the distance to the cluster (e.g., Birkinshaw 1999; Carlstrom et al. 2000). The observed microwave decrement (or more precisely, the shift of photons to higher frequencies) results as low-energy cosmic microwave background photons are scattered off the hot X-ray gas in clusters. The SZ effect is independent of distance, whereas the X-ray flux of the cluster is distance dependent; the combination thus can yield a measure of the distance.

There are also, however, a number of astrophysical complications in the practical application of this method (e.g., Birkinshaw 1999; Carlstrom 2000). For example, the gas distribution in clusters is not entirely uniform: clumping of the gas, if significant, would result in a decrease in the value of H_0. There may also be projection effects: if the clusters observed are prolate and seen end on, the true H_0 could be larger than inferred from spherical models. (In a flux-limited sample, prolate clusters could be selected on the basis of brightness.) Cooling flows may also be problematic. Furthermore, this method assumes hydrostatic equilibrium and a model for the gas and electron densities. In addition, it is vital to eliminate potential contamination from other sources. The systematic errors incurred from all of these effects are difficult to quantify.

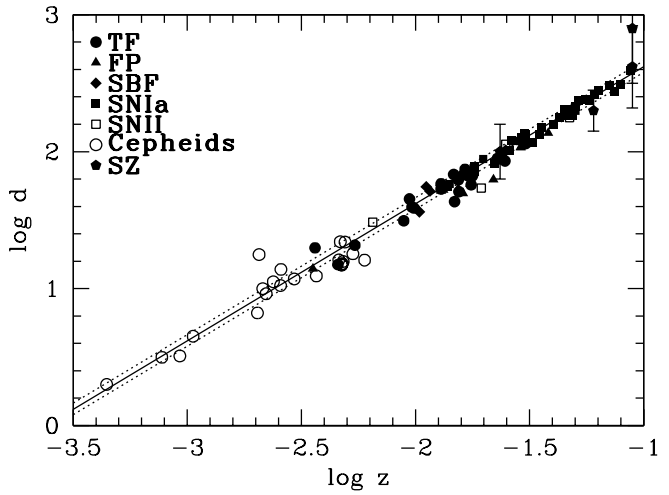

FIG. 8.—Plot of log distance in Mpc vs. log redshift for Cepheids, the Tully-Fisher relation, Type Ia supernovae, surface brightness fluctuations, fundamental plane, and Type II supernovae, calibrated as part of the Key Project. Filled circles are from Birkinshaw (1999), for nearby Sunyaev-Zeldovich clusters with $cz < 30{,}000$ ($z < 0.1$) km s^{-1}, where the choice of cosmological model does not have a significant effect on the results. The SZ clusters are Abell 478, 2142, and 2256, and are listed in Birkinshaw's Table 7. The solid line is for $H_0 = 72$ km s^{-1} Mpc^{-1}, with the dashed lines representing $\pm 10\%$.

Published values of H_0 based on the SZ method have ranged from ~ 40 to 80 km s^{-1} Mpc^{-1} (e.g., Birkinshaw 1999). The most recent two-dimensional interferometry SZ data for well-observed clusters yield $H_0 = 60 \pm 10$ km s^{-1} Mpc^{-1}. The systematic uncertainties are still large, but the near-term prospects for this method are improving rapidly (Carlstrom 2000) as additional clusters are being observed, and higher resolution X-ray and SZ data are becoming available (e.g., Reese et al. 2000; Grego et al. 2000).

9.2. *Time Delays for Gravitational Lenses*

A second method for measuring H_0 at very large distances, independent of the need for any local calibration, comes from gravitational lenses. Refsdal (1964, 1966) showed that a measurement of the time delay, and the angular separation for gravitationally lensed images of a variable object, such as a quasar, can be used to provide a measurement of H_0 (see also, e.g., the review by Blandford & Narayan 1992). Difficulties with this method stem from the fact that the underlying (luminous or dark) mass distributions of the lensing galaxies are not independently known. Furthermore, the lensing galaxies may be sitting in more complicated group or cluster potentials. A degeneracy exists between the mass distribution of the lens and the value of H_0 (Schechter et al. 1997; Romanowsky & Kochanek 1999; Bernstein & Fischer 1999). In the case of the well-studied lens 0957+561, the degeneracy due to the surrounding cluster can be broken with the addition of weak-lensing constraints. However, a careful analysis by Bernstein & Fischer emphasizes the remaining uncertainties in the mass models for both the galaxy and the cluster which dominate the overall errors in this kind of analysis. Values of H_0 based on this technique appear to be converging to about 65 km s^{-1} Mpc^{-1} (Impey et al. 1998; Tonry & Franx 1999; Bernstein & Fischer 1999; Koopmans & Fassnacht 1999; Williams & Saha 2000).

9.3. *Comparison with Other Methods*

It is encouraging that to within the uncertainties, there is broad agreement in H_0 values for completely independent techniques. A Hubble diagram (log d versus log v) is plotted in Figure 8. This Hubble diagram covers over 3 orders of magnitude, and includes distances obtained locally from Cepheids, from five secondary methods, and for four clusters with recent SZ measurements out to $z \sim 0.1$. At $z \gtrsim 0.1$, other cosmological parameters (the matter density, Ω_m, and the cosmological constant, Ω_Λ) become important.

10. IMPLICATIONS FOR COSMOLOGY

One of the classical tests of cosmology is the comparison of timescales. With a knowledge of H_0, the average density of matter, ρ, and the value of the cosmological constant, Λ, integration of the Friedmann equation

$$H^2 = \frac{8\pi G\rho}{3} - \frac{k}{r^2} + \frac{\Lambda}{3} \qquad (7)$$

yields a measure of the expansion age of the universe. This expansion age can be compared with other independent estimates of the age of the Galaxy and its oldest stars, t_0, and thus offers a test of various possible cosmological models. For example, the dimensionless product $H_0 t_0$ is $\frac{2}{3}$ in the simplest case where $\Omega_m = 1$, $\Omega_\Lambda = 0$ (the Einstein–de Sitter model), and the product is 1 for the case of an empty universe where the matter and energy density are zero.

An accurate determination of the expansion age requires not only the value of H_0, but also accurate measurements of Ω_m and Ω_Λ. At the time when the Key Project was begun, the strong motivation from inflationary theory for a flat universe, coupled with a strong theoretical preference for $\Omega_\Lambda = 0$, favored the Einstein–de Sitter model (e.g., Kolb & Turner 1990). In addition, the ages of globular cluster stars were estimated at that time to be $\sim$15 Gyr (VandenBerg, Bolte, & Stetson 1996; Chaboyer et al. 1996). However, for a value of $H_0 = 72$ km s^{-1} Mpc^{-1}, as found in this paper, the Einstein–de Sitter model yields a very young expansion age of only 9 ± 1 Gyr, significantly younger than the globular cluster and other age estimates.

Over the past several years, much progress has been made toward measuring cosmological parameters, and the Einstein–de Sitter model is not currently favored. For example, estimates of cluster velocity dispersions, X-ray masses, baryon fractions, and weak-lensing studies all have provided increasingly strong evidence for a low matter density (Ω_m) universe (e.g., Bahcall & Fan 1998). In addition, strong new evidence for a flat universe has emerged from measurements of the position of the first acoustic peak in recent cosmic microwave background anisotropy experiments (de Bernardis et al. 2000; Lange et al. 2000). Together with evidence for a low matter density, and with recent data from high-redshift supernovae (Riess et al. 1998; Perlmutter et al. 1999), evidence for a nonzero cosmological constant has been increasing. Moreover, the age estimates for globular clusters have been revised downward to 12–13 Gyr, based on a new calibration from the *Hipparcos* satellite (Chaboyer 1998; Carretta et al. 2000). A nonzero value of the cosmological constant helps to avoid a discrepancy between the expansion age and other age estimates. For $H_0 = 72$ km s^{-1} Mpc^{-1}, $\Omega_m = 0.3$, $\Omega_\Lambda = 0.7$, the expansion age is 13 ± 1 Gyr, consistent to within the uncertainties with recent globular cluster ages. In Table 15, we show expansion ages for different values of H_0 and a range of flat models.

In Figure 9 $H_0 t_0$ is plotted as a function of Ω. Two curves are shown: the solid curve is for the case where $\Lambda = 0$, and the dashed curve allows for nonzero Λ under the assumption of a flat universe. The ± 1 and 2 σ limits are plotted for $H_0 = 72$ km s^{-1} Mpc^{-1}, $t_0 = 12.5$ Gyr, assuming independent uncertainties of $\pm 10\%$ in each quantity, and adding the uncertainties in quadrature. These data are consistent with either a low-density ($\Omega_m \sim 0.1$) open universe, or a flat universe with $\Omega_m \sim 0.35$, $\Omega_\Lambda = 0.65$; however, with these data alone, it is not possible to discriminate between an open or flat universe. As described above, recent studies favor $\Omega_{\rm total} = 1$, a low matter density universe ($\Omega_m \sim 0.3$), and a nonzero value of the cosmological constant. Note, however, that the open circle at $\Omega_m = 1$, $\Lambda = 0$, represents the Einstein–de Sitter case, and is inconsistent with the current values of H_0 and t_0 only at a $\sim 2\,\sigma$ level.

TABLE 15

EXPANSION AGES (IN GYR) FOR FLAT UNIVERSES[a]

H_0/Ω_Λ	0.0	0.6	0.7	0.8
55.....	11.9	15.1	17.1	18.5
65.....	10.0	12.7	14.5	16.2
75.....	8.7	11.1	12.6	14.0
85.....	7.7	9.8	11.1	12.2

[a] $\Omega_{\rm total} = \Omega_m + \Omega_\Lambda = 1.000$.

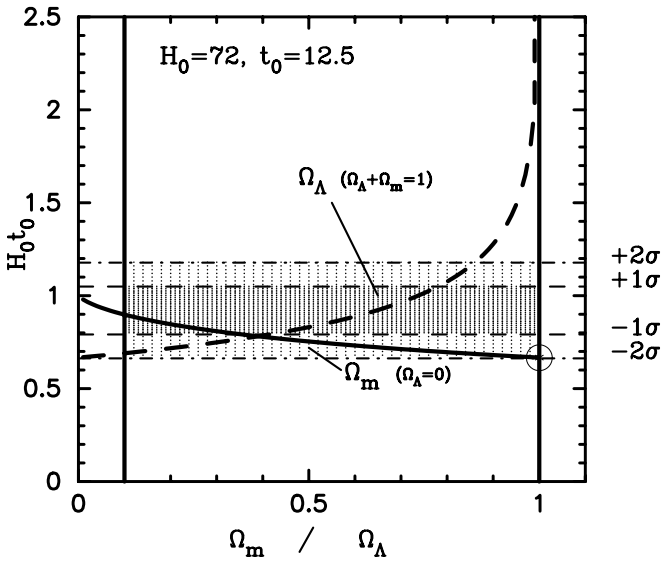

FIG. 9.—$H_0 t_0$ vs. Ω for $H_0 = 72$ km s^{-1} Mpc^{-1}, $t_0 = 12.5$ Gyr, and uncertainties of $\pm 10\%$ adopted for both quantities. The dark solid line indicates the case of a flat universe with $\Omega_\Lambda + \Omega_m = 1$. The abscissa in this case corresponds to Ω_Λ. The lighter curve represents a universe with $\Omega_\Lambda = 0$. In this case, the abscissa should be read as Ω_m. The dashed and dot-dashed lines indicate 1 and 2 σ limits, respectively, for values of $H_0 = 72$ and $t_0 = 12.5$ Gyr in the case in which both quantities are assumed to be known to $\pm 10\%$ (1 σ). The large open circle denotes values of $H_0 t_0 = \frac{2}{3}$ and $\Omega_m = 1$ (i.e., those predicted by the Einstein–de Sitter model). On the basis of a timescale comparison alone, it is not possible to discriminate between models with $\Omega_m \sim 0.1$, $\Omega_\Lambda = 0$ or $\Omega_m \sim 0.35$, $\Omega_\Lambda \sim 0.65$.

11. SUMMARY

We have used *HST* to measure Cepheid distances to 18 nearby spiral galaxies. Based on a new, larger sample of calibrating Cepheids in the Large Magellanic Cloud, an improved photometric calibration for the *HST* Wide Field and Planetary Camera 2, attention to incompleteness bias in the Cepheid period-luminosity relation, and a correction for Cepheid metallicity, we have presented here a set of self-consistent, revised Cepheid distances to 31 galaxies. The total sample includes previously published ground-based photometry, and additional *HST* studies. The *relative* Cepheid distances are determined to $\sim \pm 5\%$.

Calibrating five secondary methods with these revised Cepheid distances, we find $H_0 = 72 \pm 3 \pm 7$ km s^{-1} Mpc^{-1}, or $H_0 = 72 \pm 8$ km s^{-1} Mpc^{-1}, if we simply combine the total errors in quadrature. Type Ia supernovae currently extend out to the greatest distances, $\sim$400 Mpc. All the methods are in extremely good agreement: four of the methods yield a value of H_0 between 70 and 72 km s^{-1} Mpc^{-1}, and the fundamental plane gives $H_0 = 82$ km s^{-1} Mpc^{-1}. The largest remaining sources of error result from (1) uncertainties in the distance to the Large Magellanic Cloud, (2) photometric calibration of the *HST* Wide Field

and Planetary Camera 2, (3) metallicity calibration of the Cepheid period-luminosity relation, and (4) cosmic scatter in the density (and therefore, velocity) field that could lead to observed variations in H_0 on very large scales. A value of $H_0 = 72$ km s^{-1} Mpc^{-1} yields an expansion age of ~ 13 Gyr for a flat universe (consistent with the recent cosmic microwave background anisotropy results) if $\Omega_m = 0.3$ and $\Omega_\Lambda = 0.7$. Combined with the current best estimates of the ages of globular clusters (~ 12.5 Gyr), our results favor a Λ-dominated universe.

There are an enormous number of people who have contributed to and supported this project over the years. It is a pleasure to thank our collaborators Fabio Bresolin, Mingsheng Han, Paul Harding, Robert Hill, John Hoessel, Myung Gyoon Lee, Randy Phelps, Abhijit Saha, Kim Sebo, Nancy Silbermann, and Anne Turner for their contributions to the project. We fondly remember and acknowledge the contributions of Marc Aaronson who led our initial effort until his untimely death in 1987. Daya Rawson and Charles Prosser are also kindly remembered and missed. In particular we thank our *HST* program coordinator throughout our entire (complicated) observing process, Doug Van Orsow, and former STScI director, Robert Williams. We also thank Andrew Dolphin, Sandy Faber, Riccardo Giacconi, Riccardo Giovanelli, Jim Gunn, Martha Haynes, David Leckrone, Mark Phillips, Brian Schmidt, John Tonry, Brent Tully, and Ed Weiler. We further gratefully acknowledge the many years of assistance of the NASA and STScI support and technical staff. The work presented in this paper is based on observations with the NASA/ESA *Hubble Space Telescope*, obtained by the Space Telescope Science Institute, which is operated by AURA, Inc. under NASA contract 5-26555. Support for this work was provided by NASA through grant GO-2227-87A from STScI. This project could not have been completed in a timely fashion without the generous financial support that we received. S. M. G. H. and P. B. S. are grateful to NATO for travel support via a Collaborative Research Grant (CGR 960178). L. F. acknowledges support by NASA through Hubble Fellowship grant HF-01081.01-96A, and through grant NRA-98-03-LTSA-03. S. S. acknowledges support from NASA through the Long Term Space Astrophysics Program, NAS7-1260. B. G. acknowledges support from the NASA Long-Term Space Astrophysics Program (NAG5-7262), and the FUSE Science Team (NAS5-32985). L. M. M. acknowledges partial support through Gemini Fellowship GF-1003-95. W. L. F. acknowledges support from the NSF for the ground-based calibration in the early phases of this project under grants AST 87-13889 and AST 91-16496. This research has made use of the NASA/IPAC Extragalactic Database (NED), which is operated by the Jet Propulsion Laboratory, Caltech, under contract to the National Aeronautics and Space Administration.

APPENDIX

MAGNITUDE-LIMITED BIAS

We present here an analytic derivation of the bias introduced into the PL fits imposed by magnitude-limited cuts on extragalactic Cepheid samples. We note that in § 3.4, the application of short-period cuts to the observed PL relations (to compensate for this bias) resulted in slightly increased moduli. Depending on the sample size and its period distribution, these empirical corrections ranged from $<1\%$ up to 4% in distance. We now provide an analytic solution to reinforce our understanding of the degree and direction of this bias.

Consider Figure 10, which is meant to represent a uniform distribution of Cepheids defining a period-luminosity relation of finite width CD. It is clear that the data set defined by the parallelogram ABMN will be unbiased with respect to a fit EF (*dashed ridgeline*), where EF has the predefined slope. It is fitted to the data distribution within ABMN using least squares, assuming that all of the variance is in the vertical direction, and that errors on the periods are negligible.

Now if a magnitude-limiting cutoff to the Cepheid data is imposed (by line GH), it is clear that an asymmetry in the data distribution will be introduced with a bias in the fitted zero point ensuing: the region ACD is uncompensated for by the exclusion of its complementary region ADB. Of course, the full bias introduced by ACD will depend on the relative numbers

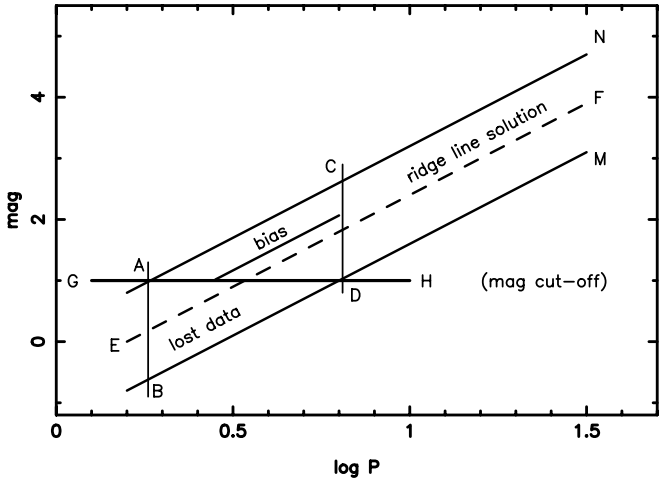

FIG. 10.—Illustration of bias due to a magnitude cutoff in the Cepheid period-luminosity relation. See text for details.

of stars in this section as compared to those in the unbiased area. However, if the section ACD is uniformly populated it can be shown that a fixed-slope solution (to that portion only) fitted by least squares would introduce a bias toward brighter magnitudes by an amount $\Delta m = w/6$, where w is the full magnitude width (measured at fixed period) of the instability strip.

The minimization of the least-squares conditioning,

$$\frac{\partial}{\partial x_0}\left[\int_0^w \left(1.0 - \frac{x}{w}\right)(x - x_0)^2\, dx\right] = 0$$

gives $x_0 = w/3$ such that the difference between the biased solution x_0 and the unbiased solution at $w/2$ is $x_0 - w/2 = -w/6$.

For the reddening-free W-PL relation, where the Key Project fitting is done, the intrinsic scatter in the relation is $\sigma = 0.08$ mag (Udalski et al. 1999), giving $w = 4\sigma \sim 0.3$ mag, and a predicted (maximum) bias of 0.05 mag, or less than about 3% in distance. This bias term will of course be diluted in direct proportion to the relative numbers of stars outside the biased zone. This is in complete agreement with the quantitative corrections found in the main text, where the typical correction is +0.02 mag, with the largest correction leading to an increase of 4% in distance.

REFERENCES

Aaronson, M., Bothun, G. D., Mould, J. R., Huchra, J., Schommer, R. A., & Cornell, M. E. 1986, ApJ, 302, 536
Aaronson, M., & Mould, J. R. 1986, ApJ, 303, 1
Aaronson, M., Mould, J. R., & Huchra, J. 1979, ApJ, 229, 1
Aaronson, M., et al. 1982, ApJS, 50, 241
Alibert, Y., Baraffe, I., Hauschildt, P., & Allard, F. 1999, A&A, 344, 551
Bahcall, N. A., & Fan, X. 1998, Proc. Natl. Acad. Sci., 95, 5956
Bernstein, G., & Fischer, P. 1999, AJ, 118, 14
Birkinshaw, M. 1999, Phys. Rep., 310, 97
Blandford, R., & Narayan, R. 1992, ARA&A, 30, 311
Bono, G., Caputo, F., Castellani, V., & Marconi, M. 1999, ApJ, 512, 711
Bono, G., Castellani, V., & Marconi, M. 2000, ApJ, 529, 293
Caputo, F., Marconi, M., Musella, I., & Santolamazza, P. 2000, A&A, 359, 1059
Cardelli, J. A., Clayton, G. C., & Mathis, J. S. 1989, ApJ, 345, 245
Carlstrom, J., et al. 2000, in Particle Physics and the Universe, ed. L. Bergstrom, P. Carlson, & C. Fransson (Singapore: World Scientific), in press
Carretta, E., Gratton, R., Clementini, G., & Fusi Pecci, F. 2000, ApJ, 533, 215
Chaboyer, B., Demarque, P., Kernan, P. J., & Krauss, L. M. 1996, Science, 271, 957
———. 1998, apJ, 494, 96
Chiosi. C., Wood, P. R., & Capitanio, N. 1993, ApJS, 86, 541
Dale, D. A., Giovanelli, R., Haynes, M. P., Campusano, L. E., & Hardy, E. 1999, AJ, 118, 1489
de Bernardis, P., et al. 2000, Nature, 404, 955
Djorgovski, G., & Davis, M. 1987, ApJ, 313, 59
Dolphin, A. 2000, PASP, 112, 1397
Dressler, A., Lynden-Bell, D., Burstein, D., Davies, R. L., Faber, S. M., Terlevich, R., & Wegner, G. 1987, ApJ, 313, 42
Eastman, R. G., Schmidt, B. P., & Kirshner, R. 1996, ApJ, 466, 911
Evans, N. R. 1995, ApJ, 445, 393
Faber, S. M., & Jackson, R. E. 1976, ApJ, 204, 668
Feast, M. W., & Catchpole, R. M. 1997, MNRAS, 286, 1L
Feast, M., & Walker, A. R. 1987, ARA&A, 25, 345
Ferrarese, L., et al. 1996, ApJ, 464, 568
———. 1998, ApJ, 507, 655
———. 2000a, ApJ, 529, 745
———. 2000b, ApJS, 128, 431
Ferrarese, L., Silbermann, N. A., Mould, J. R., Stetson, P. B., Saha, A., Freedman, W. L., & Kennicutt, R. C. 2000c, PASP, 112, 177
Freedman, W. L. 1988, ApJ, 326, 691
———. 1990, ApJ, 355, L35
———. 1997, in Critical Dialogs in Cosmology, ed. N. Turok (Singapore: World Scientific), 92
———. 2000a, in Particle Physics and the Universe, ed. L. Bergstrom, P. Carlson, & C. Fransson (Singapore: World Scientific), in press (preprint astro-ph/9905222)
———. 2000b, Phys. Rep., 333, 13
Freedman, W. L., & Madore, B. F. 1988, ApJ, 322, 63
———. 1990, ApJ, 365, 186
———. 1996, in ASP Conf. Ser. 88, Clusters, Lensing and the Future of the Universe, ed. V. Trimble & A. Reisenegger (San Francisco: ASP), 9
Freedman, W. L., Madore, B. F., Hawley, S. L., Horowitz, I. K., Mould, J., Navarrete, M., & Sallmen, S. 1992, ApJ, 396, 80
Freedman, W. L., Wilson, C. D., & Madore, B. F. 1991, ApJ, 372, 455
Freedman, W. L., et al. 1994a, Nature, 371, 757
———. 1994b, ApJ, 427, 628
Gelman, A., Carlin, J. B., Stern, H. S., & Rubin, D. B. 1995, Bayesian Data Analysis (London: Chapman & Hall)
Gibson, B. K. 2000, Mem. Soc. Astron. Italiana, in press (preprint astro-ph/9910574)
Gibson, B. K., Maloney, P. R., & Sakai, S. 2000a, ApJ, 530, L5
Gibson, B. K., et al. 1999, ApJ, 512, 48
———. 2000b, ApJ, 529, 723
Giovanelli, R., Dale, D. A., Haynes, M. P., Hardy, E., & Campusano, L. E. 1999, ApJ, 525, 25
Giovanelli, R., Haynes, M. P., Salzer, J. J., Wegner, G., Da Costa, L. N., & Freudling, W. 1998, AJ, 116, 2632
Giovanelli, R., Haynes, M. P., Vogt, N. P., Wegner, G., Salzer, J. J., Da Costa, L. N., & Freudling, W. 1997, AJ, 113, 22
Graham, J. A., et al. 1997, ApJ, 477, 535
———. 1999, ApJ, 516, 626
Grego, L., Carlstrom, J. E., Joy, M. K., Reese, E. D., Holder, G. P., Patel, S., Cooray, A. R., & Holzapfel, W. L. 2000, ApJ, 539, 39
Groenewegen, M. A. T., & Oudmaijer, R. D. 2000, A&A, 356, 849
Hamuy, M., Phillips, M. M., Maza, J., Suntzeff, N. B., Schommer, R. A., & Aviles, R. 1995, AJ, 109, 1
Hamuy, M., Phillips, M. M., Suntzeff, N. B., & Schommer, R. A. 1996, AJ, 112, 2398
Han, M., & Mould, J. R. 1990, ApJ, 360, 448
Herrnstein, J. R., Moran, J. M., Greenhill, L. J., Diamond, P. J., Inoue, M., Nakai, N., Miyoshi, M., Henkel, C., & Riess, A. 1999, Nature, 400, 539
Hill, R. J., et al. 1998, ApJ, 496, 648
Hubble, E. P. 1929, Publ. Nat. Acad. Sci., 15, 168
Hughes, S. M. G., et al. 1998, ApJ, 501, 32
Impey, C. D., et al. 1998, ApJ, 509, 551
Jacoby, G. H., et al. 1992, PASP, 104, 599
Jha, S., et al. 1999, ApJS, 125, 73
Jorgensen, I., Franx, M., & Kjaergaard, P. 1996, MNRAS, 280, 167
Kelson, D. D., et al. 1996, ApJ, 463, 26
———. 1999, ApJ, 514, 614
———. 2000, ApJ, 529, 768
Kennicutt, R. C., Jr., Freedman, W. L., & Mould, J. R. 1995, AJ, 110, 1476
Kennicutt, R. C., Jr., et al. 1998, ApJ, 498, 181
Kochanek, C. S. 1997, ApJ, 491, 13
Kolb, E. W., & Turner, M. S. 1990, The Early Universe (New York: Addison-Wesley)
Koopmans, L. V. E., & Fassnacht, C. D. 1999, ApJ, 527, 513
Kowal, C. T. 1968, AJ, 73, 1021
Lange, A. E., et al. 2000, Phys. Rev. D, 63, 042001
Lauer, T. R., & Postman, M. 1992, ApJ, 400, L47
Lauer, T. R., Tonry, J. L., Postman, M., Ajhar, E. A., & Holtzman, J. A. 1998, ApJ, 499, 577
Macri, L. M., Huchra, J. P., Sakai, S., Mould, J. R., & Hughes, S. M. G. 2000, ApJS, 128, 461
Macri, L. M., et al. 1999, ApJ, 521, 155
———. 2001, ApJ, in press
Madore, B. F. 1982, ApJ, 253, 575
Madore, B. F., & Freedman, W. L. 1991, PASP, 103, 933
———. 1998, ApJ, 492, 110
Madore, B. F., et al. 1998, Nature, 395, 47
———. 1999, ApJ, 515, 29
Maoz, E., Newman, J., Ferrarese, L., Davis, M., Freedman, W. L., Madore, B. F., Stetson, P. B., & Zepf, S. 1999, Nature, 401, 351
McGaugh, S., Schombert, J., Bothun, G., & de Blok, E. 2000, ApJ, 533, L99
Mochejska, B. J., Macri, L. M., Sasselov, D. D., & Stanek, K. Z. 2000, AJ, 120, 810
Mochejska, B. J., et al. 2001, BAAS, 197, 104.03
Mould, J. R., Sakai, S., Hughes, S., & Han, M. 1996, in The Extragalactic Distance Scale, ed., M. Livio, M. Donahue, & N. Panagia (Cambridge: Cambridge Univ. Press), 158
Mould, J. R., et al. 2000a, ApJ, 529, 786 (erratum 545, 547)
———. 2000b, ApJ, 528, 655
Newman, J. A., Ferrarese, L., Stetson, P. B., Maoz, E., Zepf, E., Davis, M., Freedman, W. L., & Madore, B. F. 2001, ApJ, in press
Parodi, B. F., Saha, A., Sandage, A., & Tammann, G. A. 2000, ApJ, 540, 634
Peacock, J. A. 1999, Cosmological Physics (Cambridge: Cambridge Univ. Press)
Perlmutter, S., et al. 1999, ApJ, 517, 565
Phelps, R. L., et al. 1998, ApJ, 500, 763

Phillips, M. M., Lira, P., Suntzeff, N. B., Schommer, R. A., Hamuy, M., & Maza, J. 1999, AJ, 118, 1766
Pierce, M. J., & Tully, R. B. 1988, ApJ, 330, 579
Press, W. H. 1997, in Unsolved Problems in Astrophysics, ed. J. N. Bahcall & J. P. Ostriker (Princeton: Princeton Univ. Press), 49
Prosser, C. F., et al. 1999, ApJ, 525, 80
Rawson, D. M., et al. 1997, ApJ, 490, 517
Reese, E. D., et al. 2000, ApJ, 533, 38
Refsdal, S. 1964, MNRAS, 128, 295
———. 1966, MNRAS, 132, 101
Riess, A. G., et al. 1998, AJ, 116, 1009
———. 1999, AJ, 117, 707
Romanowsky, A. J., & Kochanek, C. S. 1999, ApJ, 516, 18
Saha, A., Labhardt, L., & Prosser, C. 2000, PASP, 112, 163
Saha, A., Sandage, A. R., Labhardt, L., Schwengeler, H., Tammann, G. A., Panagia, N., & Macchetto, F. D. 1995, ApJ, 438, 8
Saha, A., Sandage, A. R., Labhardt, L., Tammann, G. A., Macchetto, F. D., & Panagia, N. 1996, ApJ, 466, 55
———. 1997, ApJ, 486, 1
———. 1999, ApJ, 522, 802
Sakai, S., et al. 1999, ApJ, 523, 540
———. 2000, ApJ, 529, 698
Sandage, A. 1988, PASP, 100, 935
Sandage, A. R., & Bedke J. 1988, Atlas of Galaxies Useful for Measuring the Cosmological Distance Scale (NASA SP-496; Washington: NASA)
Sandage, A. R., Bell, R. A., & Tripicco, M. J. 1999, ApJ, 522, 250
Sandage, A. R., & Hardy, E. 1973, ApJ, 183, 743
Sandage, A. R., Saha, A., Tammann, G. A., Labhardt, L., Panagia, N., & Macchetto, F. D. 1996, ApJ, 460, L15
Sandage, A., & Tammann, G. A. 1982, ApJ, 256, 339
Sasselov, D. D., et al. 1997, A&A, 324, 471
Schechter, P. 1980, AJ, 85, 801
Schechter, P., Mateo, M., & Saha, A. 1993, PASP, 105, 1342
Schechter, P., et al. 1997, ApJ, 475, L85
Schlegel, D. J., Finkbeiner, D. P., & Davis, M. 1998, ApJ, 500, 525
Schmidt, B. P., Eastman, R. G., & Kirshner, R. 1994, ApJ, 432, 42
Shi, X., & Turner, M. S. 1998, ApJ, 493, 519
Silbermann, N. A., et al. 1996, ApJ, 470, 1
———. 1999, ApJ, 515, 1
Stanek, K. Z., Kaluzny, J., Wysocka, A., & Thompson, I. 2000, Acta Astron., 50, 191
Stanek, K. Z., & Udalski, A. 1999, ApJL, submitted (preprint astro-ph/9909346)
Steinmetz, M., & Navarro, J. F. 1999, ApJ, 513, 555
Stetson, P. B. 1994, PASP, 106, 250
———. 1996, PASP, 108, 851 (TRIAL)
———. 1998, PASP, 110, 1448
Suntzeff, N. B., et al. 1999, AJ, 117, 1175
Tanvir, N. R. 1999, in ASP Conf. Ser. 167, Harmonizing Cosmic Distance Scales in a Post-*Hipparcos* Era, ed. D. Egret & A. Heck (San Francisco: ASP), 84
Tanvir, N. R., Ferguson, H. C., & Shanks, T. 1999, MNRAS, 310, 175
Tanvir, N. R., Shanks, T., Ferguson, H. C., & Robinson, D. R. T. 1995, Nature, 377, 27
Tonry, J. L. 1991, ApJ, 373, L1
Tonry, J. L., Blakeslee, J. P., Ajhar, E. A., & Dressler, A. 1997, ApJ, 475, 399
———. 2000, ApJ, 530, 625
Tonry, J. L., & Franx, M. 1999, ApJ, 515, 512
Tonry, J. L., & Schneider, D. 1988, AJ, 96, 807
Tully, R. B., & Fisher, J. R. 1977, A&A, 54, 661
Tully, R. B., & Pierce, M. J. 2000, ApJ, 533, 744
Turner, A., et al. 1998, ApJ, 505, 207
Turner, E. L., Cen, R., & Ostriker, J. P. 1992, AJ, 103, 1427
Udalski, A. 2000, ApJ, 531, L25
Udalski, A., Szymanski, M., Kubiak, M., Pietrzynski, G., Soszynski, I., Wozniak, P., & Zebrun, K. 1999, Acta Astron., 49, 201
VandenBerg, D. A., Bolte, M., & Stetson, P. B. 1996, ARA&A, 34, 461
Walker, A. R. 1999, in Post-*Hipparcos* Cosmic Candles (Dordrecht: Kluwer), 125
Wang, Y., Spergel, D. N., & Turner, E. L. 1998, ApJ, 498, 1
Westerlund, B. E. 1997, in The Magellanic Clouds (Cambridge: Cambridge Univ. Press)
Whitmore, B., Heyer, I., & Casertano, S. 1999, PASP, 111, 1559
Williams, L. L. R., & Saha, P. 2000, AJ, 119, 439
Willick, J. A. 1994, ApJS, 92, 1
Willick, J. A., & Batra, P. 2001, ApJ, 548, 564
Zaritsky, D., Kennicutt, R. C., Jr., & Huchra, J. P. 1994, ApJ, 420, 87
Zehavi, I., Riess, A. G., Kirshner, R. P., & Dekel, A. 1998, ApJ, 503, 483